

Massive Star Formation

Jonathan C. Tan¹, Maria T. Beltrán², Paola Caselli³, Francesco Fontani², Asunción Fuente⁴,
Mark R. Krumholz⁵, Christopher F. McKee⁶, Andrea Stolte⁷

¹University of Florida; ²INAF-Osservatorio Astrofisico di Arcetri; ³University of Leeds; ⁴Observatorio Astronómico Nacional;
⁵University of California, Santa Cruz; ⁶University of California, Berkeley; ⁷Argelander Institut für Astronomie, Universität Bonn

The enormous radiative and mechanical luminosities of massive stars impact a vast range of scales and processes, from the reionization of the universe, to the evolution of galaxies, to the regulation of the interstellar medium, to the formation of star clusters, and even to the formation of planets around stars in such clusters. Two main classes of massive star formation theory are under active study, *Core Accretion* and *Competitive Accretion*. In Core Accretion, the initial conditions are self-gravitating, centrally concentrated cores that condense with a range of masses from the surrounding, fragmenting clump environment. They then undergo relatively ordered collapse via a central disk to form a single star or a small- N multiple. In this case, the pre-stellar core mass function has a similar form to the stellar initial mass function. In Competitive Accretion, the material that forms a massive star is drawn more chaotically from a wider region of the clump without passing through a phase of being in a massive, coherent core. In this case, massive star formation must proceed hand in hand with star cluster formation. If stellar densities become very high near the cluster center, then collisions between stars may also help to form the most massive stars. We review recent theoretical and observational progress towards understanding massive star formation, considering physical and chemical processes, comparisons with low and intermediate-mass stars, and connections to star cluster formation.



NOT APPROVED

1. INTRODUCTION

Across the universe, massive stars play dominant roles in terms of their feedback and their synthesis and dispersal of heavy elements. Achieving a full theoretical understanding of massive star formation is thus an important goal of contemporary astrophysics. This effort can also be viewed as a major component of the development of a general theory of star formation that seeks to explain the birth of stars of all masses and from all varieties of star-forming environments.

Two main classes of theory are under active study, *Core Accretion* and *Competitive Accretion*. In Core Accretion, extending “standard” low-mass star formation theory (*Shu et al.*, 1987), the initial conditions are self-gravitating, centrally concentrated *cores* of gas that condense with a range of masses from a fragmenting *clump* (i.e., protocluster) environment. These cores then undergo gravitational collapse via a central disk, to form a single star or small- N multiple. The pre-stellar core (PSC) mass function (CMF) has a shape similar to the stellar initial mass function (IMF). In Competitive Accretion, gas that forms a massive star is drawn chaotically from a wider region of the clump, without ever being in a massive, coherent, gravitationally bound, starless core. Also, a forming massive star is always surrounded by a swarm of low-mass protostars. Competitive Accretion is sometimes said to lead naturally to the IMF (*Bonnell et al.*, 2001; 2007): then the total mass of massive stars must be a small fraction of the total stellar mass formed from the clump. If the density of protostars congregating near the cluster center becomes sufficiently high, then stellar collisions may also assist in forming the most massive stars.

Recent advances in theoretical/numerical modeling of massive star formation involve inclusion of more physical processes, like radiation pressure, magnetic fields and protostellar outflows. Observationally, progress has resulted from telescopes such as *Spitzer*, *Herschel*, *SOFIA*, *ALMA* and the *VLA*. Galactic plane surveys have yielded large samples of candidate massive protostars and their birth clouds.

This review aims to summarize massive star formation research, focusing on developments since the reviews of *Beuther et al.* (2007), *Zinnecker and Yorke* (2007) and *McKee & Ostriker* (2007). We do not discuss formation of the first stars, which are thought to have been massive (e.g., *Bromm*, 2013). Given the complexity of massive star formation, detailed comparison of theoretical predictions with observational results is needed for progress in understanding which accretion mechanism(s) is relevant and which physical and chemical processes are important. We thus first overview basic observed properties of massive star-forming regions (§1.1), which set boundary conditions on theoretical models. Next we present a theoretical overview of physical processes likely involved in forming massive stars (§2), including the different accretion models, protostellar evolution and feedback, and results from numerical simulations. We then focus on observational results on the earlier, i.e., initial condition (§3) and later, i.e., accretion (§4) stages of massive star formation. Here we discuss astrochemical modeling, as well as general comparisons of massive star formation with intermediate/low-mass star formation. The relation of massive star formation to star cluster formation is examined in §5. We conclude in §6.

1.1. The Birth Environments of Massive Stars

The basic physical properties of regions observed to be forming or have formed massive stars, i.e., gas clumps and young star clusters, are shown in Fig. 1, plotting mass surface density, $\Sigma = M/(\pi R^2)$, of the structure versus its mass, M . Stars, including massive stars, form in molecular gas, that is mostly found in giant molecular clouds (GMCs) with $\Sigma \sim 0.02 \text{ g cm}^{-2}$. Note $1.0 \text{ g cm}^{-2} \equiv 4790 M_\odot \text{ pc}^{-2}$, for which $N_{\text{H}} = 4.27 \times 10^{23} \text{ cm}^{-2}$ (assuming $n_{\text{He}} = 0.1 n_{\text{H}}$ so mass per H is $\mu_{\text{H}} = 2.34 \times 10^{-24} \text{ g}$) and visual extinction is $A_V = (N_{\text{H}}/2.0 \times 10^{21} \text{ cm}^{-2}) \text{ mag} = 214 \text{ mag}$. However, star formation is seen to be localized within star-forming clumps within GMCs, which typically have $\Sigma_{\text{cl}} \sim 0.1 - 1 \text{ g cm}^{-2}$. Some massive systems, usually already-formed star clusters, have Σ up to $\sim 30 \text{ g cm}^{-2}$.

In terms of Σ_{cl} (in g cm^{-2}) and $M_{\text{cl},3} = M_{\text{cl}}/(1000 M_\odot)$, the radius and (H number) density of a spherical clump are

$$R_{\text{cl}} = 0.258 M_{\text{cl},3}^{1/2} \Sigma_{\text{cl}}^{-1/2} \text{ pc}, \quad (1)$$

$$\bar{n}_{\text{H,cl}} = 4.03 \times 10^5 \Sigma_{\text{cl}}^{3/2} M_{\text{cl},3}^{-1/2} \text{ cm}^{-3}. \quad (2)$$

Gas clumps massive enough to form a cluster of mass $M_{*\text{cl}} \sim 500 M_\odot$, i.e., with median expected maximum stellar mass $\sim 30 M_\odot$ (for Salpeter IMF from 0.1 to $120 M_\odot$), are thus $\sim 0.3 \text{ pc}$ in size (if $\Sigma_{\text{cl}} \sim 1 \text{ g cm}^{-2}$ and efficiency $\epsilon_{*\text{cl}} \equiv M_{*\text{cl}}/M_{\text{cl}} \sim 0.5$), only moderately larger than the $\sim 0.1 \text{ pc}$ sizes of well-studied low-mass starless cores in regions such as Taurus (*Bergin and Tafalla, 2007*). However, mean densities in such clumps are at least ten times larger.

2. THEORETICAL OVERVIEW

2.1. Physical Processes in Self-Gravitating Gas

The importance of self-gravity in a cloud of mass M and radius R can be gauged by the virial parameter

$$\alpha_{\text{vir}} \equiv 5\sigma^2 R/(GM) = 2aE_K/E_G, \quad (3)$$

where σ is 1D mass-averaged velocity dispersion, $a \equiv E_G/(3GM^2/[5R])$ is the ratio of gravitational energy, E_G (assuming negligible external tides), to that of a uniform sphere, and E_K is the kinetic energy (*Bertoldi and McKee, 1992*). Often α_{vir} is set as $2E_K/E_G$, with the advantage of clearly denoting bound ($E_K < E_G$) and virialized ($E_K = \frac{1}{2}E_G$) clouds, but the disadvantage that a is difficult to observe. For spherical clouds with a power-law density distribution, $\rho \propto r^{-k_\rho}$, a rises from 1 to $\frac{5}{3}$ as k_ρ goes from 0 (uniform density) to 2 (singular isothermal sphere). A cloud in free-fall has $\alpha_{\text{vir}} \rightarrow 2a$ from below as time progresses. The cloud's escape velocity is $v_{\text{esc}} = (10/\alpha_{\text{vir}})^{1/2} \sigma$.

The velocity dispersion in a cloud is thus given by

$$\sigma \equiv (\pi \alpha_{\text{vir}} G \Sigma R / 5)^{1/2}, \quad (4)$$

where we have used the identity symbol to emphasize that this follows from the definition of α_{vir} . Clouds that are gravitationally bound with $\alpha_{\text{vir}} \sim 1$ and that have similar surface densities, then naturally satisfy a line-width

size (LWS) relation $\sigma \propto R^{1/2}$ (*Larson, 1985*), consistent with observations (*McKee and Ostriker, 2007; Heyer et al., 2009*). *McKee et al.* (2010) termed this the virialized LWS relation for $\alpha_{\text{vir}} = 1$, as suggested by *Heyer et al.* (2009). By contrast, the standard turbulence-dominated LWS relation, $\sigma = \sigma_{\text{pc}} R_{\text{pc}}^{1/2}$, where $\sigma_{\text{pc}} \simeq 0.72 \text{ km s}^{-1}$ in the Galaxy (*McKee and Ostriker, 2007*), is independent of Σ . The virialized LWS relation applies for mass surface densities $\Sigma > \Sigma_{\text{LWS}} = (5/[\pi G])(\sigma_{\text{pc}}^2/1 \text{ pc}) \simeq 0.040 \text{ g cm}^{-2}$. Since regions of massive star formation have column densities substantially greater than this, they lie above the turbulence-dominated LWS relation, as observed (*Plume et al., 1997*).

Evaluating eq. (4) for massive star-forming regions,

$$\sigma = 1.826 \alpha_{\text{vir}}^{1/2} (M_3 \Sigma)^{1/4} \text{ km s}^{-1}, \quad (5)$$

yields supersonic motions, as the isothermal sound speed $c_{\text{th}} = 0.188(T/10 \text{ K})^{1/2} \text{ km s}^{-1}$ and $T \lesssim 30 \text{ K}$ for gas not too close to a massive star. These motions cannot be primarily infall, since clump infall (§4.1) and star-formation rates per free-fall time are quite small (*Krumholz and Tan, 2007*). It is therefore likely that regions of massive star formation are dominated by supersonic turbulence. If so, then the gas inside a clump of radius R_{cl} will obey a LWS relation $\sigma = (R/R_{\text{cl}})^q \sigma_{\text{cl}}$ with $q \leq \frac{1}{2}$ (*Matzner, 2007*), so

$$\alpha_{\text{vir}} = (5/\pi)(\sigma_{\text{cl}}^2/[R_{\text{cl}}G\Sigma]) = (\Sigma_{\text{cl}}/\Sigma)\alpha_{\text{vir,cl}}. \quad (6)$$

At a typical point in the clump, the density is less than average, so α_{vir} of a sub-region of size R is $> (R_{\text{cl}}/R)\alpha_{\text{vir,cl}}$. Even if the clump is bound, the sub-region is not. However, for $q = \frac{1}{2}$, a sub-region compressed so that $\Sigma \gtrsim \Sigma_{\text{cl}}$ has $\alpha_{\text{vir}} \lesssim \alpha_{\text{vir,cl}}$ and is bound if the clump is; for $q < \frac{1}{2}$, extra compression is needed to make a bound sub-region.

Isothermal clouds more massive than the critical mass, M_{cr} , cannot be in hydrostatic equilibrium and will collapse. In this case, M_{cr} is termed the Bonnor-Ebert mass, given by

$$M_{\text{cr}} = M_{\text{BE}} = \bar{\mu}_{\text{cr}} c_{\text{th}}^3 (G^3 \bar{\rho})^{-1/2} = \bar{\mu}_{\text{cr}} c_{\text{th}}^4 (G^3 \bar{P})^{-1/2}, \quad (7)$$

where \bar{P} is mean pressure in the cloud, and $\bar{\mu}_{\text{cr}} = 1.856$ (*McKee and Holliman, 1999*; M_{cr} can also be expressed in terms of density at the cloud's surface: then $\bar{\mu}_{\text{cr}} = 1.182$). For non-magnetic clouds this relation can be generalized to an arbitrary equation of state by replacing c_{th}^2 with σ^2 . One can show that $\bar{\mu}_{\text{cr}}$ corresponds to a critical value of the virial parameter, $\alpha_{\text{vir,cr}} = 5(3/[4\pi])^{1/3} \bar{\mu}_{\text{cr}}^{-2/3}$; clouds with $\alpha_{\text{vir}} < \alpha_{\text{vir,cr}}$ will collapse. For example, equilibrium isothermal clouds have $\alpha > \alpha_{\text{vir,cr}} = 2.054$.

The critical mass associated with magnetic fields can be expressed in two ways (e.g., *McKee and Ostriker, 2007*): as $M_\Phi = \Phi/(2\pi G^{1/2})$, where Φ is the magnetic flux, or as $M_B = M_\Phi^3/M^2$, which can be rewritten as

$$M_B = (9/[16\sqrt{\pi}]) v_A^3 (G^3 \bar{\rho})^{-1/2}, \quad (8)$$

where v_A is the Alfvén velocity. Magnetically critical clouds have $M = M_\Phi = M_B$. Most regions with Zeeman observations are magnetically supercritical (*Crutcher,*

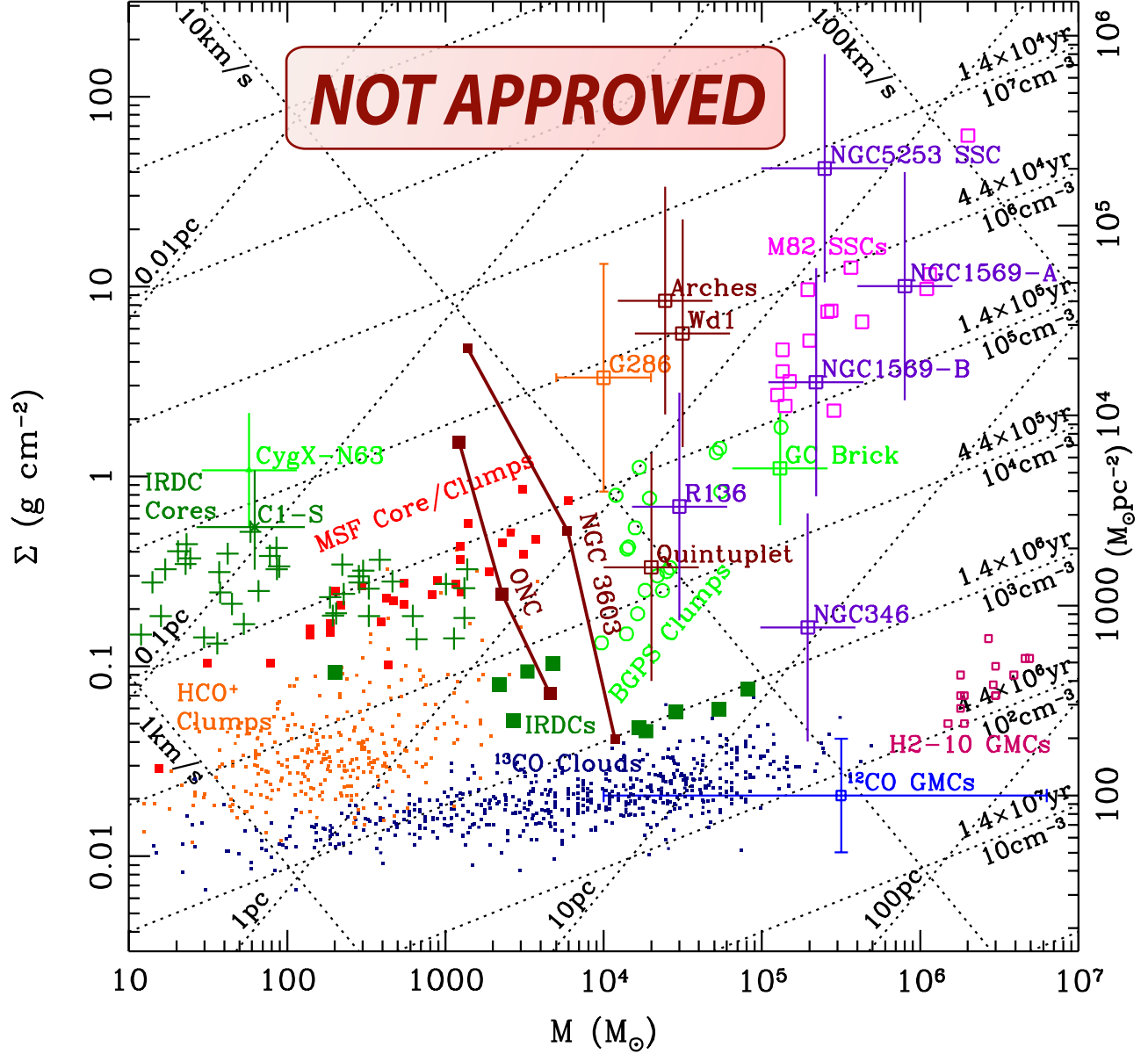


Fig. 1.— The Environments of Massive Star Formation. Mass surface density, $\Sigma \equiv M/(\pi R^2)$, is plotted versus mass, M . Dotted lines of constant radius, R , H number density, n_{H} (or free-fall time, $t_{\text{ff}} = (3\pi/[32G\rho])^{1/2}$), and escape speed, $v_{\text{esc}} = (10/\alpha_{\text{vir}})^{1/2}\sigma$, are shown. Stars form from molecular gas, which in the Galaxy is mostly organized into GMCs. Typical ^{12}CO -defined GMCs have $\Sigma \sim 100 M_{\odot} \text{pc}^{-2}$ (Solomon *et al.*, 1987) (see Tan *et al.*, 2013a for detailed discussion of the methods for estimating Σ for the objects plotted here), although denser examples have been found in Henize 2-10 (Santangelo *et al.*, 2009). The ^{13}CO -defined clouds of Roman-Duval *et al.* (2010) are indicated, along with HCO^+ clumps of Barnes *et al.*, (2011), including G286.21+0.17 (Barnes *et al.*, 2010). Along with G286, the BGPS clumps (Ginsburg *et al.*, 2012) and the Galactic Center “Brick” (Longmore *et al.*, 2012) are some of the most massive, high- Σ gas clumps known in the Milky Way. Ten example Infrared Dark Clouds (IRDCs) (Kainulainen and Tan, 2013) and their internal core/clumps (Butler and Tan, 2012) are shown, including the massive, monolithic, highly-deuterated core C1-S (Tan *et al.*, 2013b). CygX-N63, a core with similar mass and size as C1-S, appears to be forming a single massive protostar (Bontemps *et al.*, 2010; Duarte-Cabral *et al.*, 2013). The IRDC core/clumps overlap with Massive Star-Forming (MSF) core/clumps (Mueller *et al.*, 2002). Clumps may give rise to young star clusters, like the ONC (e.g., Da Rio *et al.*, 2012) and NGC 3603 (Pang *et al.*, 2013) (radial structure is shown from core to half-mass, $R_{1/2}$, to outer radius), or even more massive examples, e.g., Westerlund 1 (Lim *et al.*, 2013), Arches (Habibi *et al.*, 2013), Quintuplet (Hußmann *et al.*, 2012) (shown at $R_{1/2}$), that are in the regime of “super star clusters” (SSCs), i.e., with $M_{*} \gtrsim 10^4 M_{\odot}$. Example SSCs in the Large Magellanic Cloud (LMC) (R136, Andersen *et al.*, 2009) and Small Magellanic Cloud (SMC) (NGC 346, Sabbi *et al.*, 2008) display a wide range of Σ , but no evidence of IMF variation (§5.2). Even more massive clusters can be found in some dwarf irregular galaxies, such as NGC 1569 (Larsen *et al.*, 2008) and NGC 5253 (Turner and Beck, 2004), and starburst galaxy M82 (McCradly and Graham, 2007).

2012); i.e., $M > M_\Phi$ so that the field, on its own, cannot prevent collapse. Magnetized isothermal clouds have $M_{\text{cr}} \simeq M_{\text{BE}} + M_\Phi$, and since most GMCs are gravitationally bound (e.g., *Roman-Duval et al.*, 2010; *Tan et al.*, 2013a), magnetized and turbulent, they are expected to have $M \simeq M_{\text{cr}} \simeq 2M_\Phi$ (*McKee*, 1989). Magnetically subcritical clouds can evolve to being supercritical by flows along field lines and/or by ambipolar diffusion. In a quiescent medium, the ambipolar diffusion time is about 10 free-fall times (*Mouschovias*, 1987); this time scale is reduced in the presence of turbulence (e.g., *Fatuzzo and Adams*, 2002; *Li et al.*, 2012b). Lazarian and collaborators (e.g., *de Gouveia Dal Pino et al.*, 2012 and references therein) have suggested super-Alfvénic turbulence drives rapid reconnection that can efficiently remove magnetic flux from a cloud.

Self-gravitating clouds in virial equilibrium have a mean total pressure (thermal, turbulent and magnetic) that is related to the total Σ via (*McKee and Tan*, 2003 [MT03]),

$$\bar{P} \equiv (3\pi/20)f_g\phi_{\text{geom}}\phi_B\alpha_{\text{vir}}G\Sigma^2, \quad (9)$$

where f_g is the fraction of total mass surface density in gas (as opposed to stars), ϕ_{geom} is an order unity numerical factor that accounts for the effect of nonspherical geometry, $\phi_B \simeq 1.3 + 3/(2\mathcal{M}_A^2)$ accounts for the effect of magnetic fields, and $\mathcal{M}_A = \sqrt{3}(\sigma/v_A)$ is the Alfvén Mach number. A magnetized cloud with the same total pressure and surface density as a non-magnetic cloud will therefore have a virial parameter that is smaller by a factor ϕ_B . Clouds that are observed to have small α_{vir} (e.g., *Pillai et al.*, 2011; see also §3.1) are therefore either in the very early stages of gravitational collapse or are strongly magnetized.

The characteristic time for gravitational collapse is the free-fall time. For a spherical cloud, this is

$$\bar{t}_{\text{ff}} = (3\pi/[32G\bar{\rho}])^{1/2} = 6.85 \times 10^4 M_3^{1/4} \Sigma^{-3/4} \text{ yr}, \quad (10)$$

where the bar on t_{ff} indicates that it is given in terms of the mean density of the mass M . The free-fall velocity is

$$v_{\text{ff}} = (2GM/r)^{1/2} = 5.77(M_3\Sigma)^{1/4} \text{ km s}^{-1}. \quad (11)$$

An isothermal filament with mass/length $m_\ell > 2c_{\text{th}}^2/G = 16.4(T/10 \text{ K}) M_\odot \text{ pc}^{-1}$ cannot be in equilibrium and will collapse. Its free-fall time and velocity are $(1/2)(G\bar{\rho})^{-1/2}$ and $2[Gm_\ell \ln(r_0/r)]^{1/2} = 1.3[m_{\ell,100} \ln(r_0/r)]^{1/2} \text{ km s}^{-1}$, with r_0 the initial radius of collapsing gas and $m_{\ell,100} = m_\ell/100 M_\odot \text{ pc}^{-1}$. Infall velocities much less than this indicate either collapse has just begun or that it is quasi-static.

2.2. Formation Mechanisms

A key parameter in both Core and Competitive Accretion is the characteristic accretion rate in a cloud with $M \geq M_{\text{cr}}$,

$$\dot{m}_{\text{ff}} = M/\bar{t}_{\text{ff}} = (8G/\sqrt{\pi})^{1/2}(M\Sigma)^{3/4}, \quad (12)$$

$$= 1.46 \times 10^{-2}(M_3\Sigma)^{3/4} M_\odot \text{ yr}^{-1}. \quad (13)$$

In Competitive Accretion models, the star-forming clump undergoes global, typically free-fall, collapse, so this is the

characteristic accretion rate in the entire forming cluster. In Core Accretion models, this is the characteristic accretion rate to the central star and disk in the core, with the accreted gas then supplied to just one or a few protostars. The properties of the surrounding clump are assumed to be approximately constant during the formation of the star.

The corresponding accretion time, $t_{\text{acc}} \propto M/\dot{m}_{\text{ff}} \propto \bar{t}_{\text{ff}} \propto M^{1/4}$, is a weak function of mass for clouds of a given Σ . Note, a singular isothermal sphere has $\rho \propto r^{-2}$ so its collapse leads to $\dot{m}_{\text{ff}} \propto (M\Sigma)^{3/4} = \text{const}$ (*Shu*, 1977).

2.2.1. Core Accretion

The principal assumption of Core Accretion models is that the initial conditions for intermediate and massive star formation are gravitationally bound cores, scaled up in mass from the low-mass examples known to form low-mass stars. Different versions of these models invoke varying properties of the cores, including their expected densities, density profiles, sources of internal pressure and dynamical states. A distinguishing feature of these models is that the pre-stellar CMF is hypothesized to be similar in shape to the stellar IMF, with stellar masses being $m_* = \epsilon_c M_c$, where $\epsilon_c \sim 0.5$, perhaps set by protostellar outflow feedback (*Matzner and McKee*, 2000; see §2.4). This feature of some kind of one-to-one correspondence between the CMF and IMF is an underlying assumption of recent theories of the IMF, which predict the CMF based on the conditions needed to form bound cores in a turbulent medium (e.g., *Padoan and Nordlund*, 2007; cf., *Clark et al.*, 2007).

There are at least two main differences between low and high-mass star formation: First, for sufficiently massive stars, the Kelvin-Helmholtz time can be less than the accretion time, so the star accretes while on the main sequence (*Kahn*, 1974). Second, cores forming massive stars are large enough that internal turbulence can dominate thermal motions (*Myers and Fuller*, 1992; *Caselli and Myers*, 1995). Extending the work of these authors, *McKee and Tan* (2002; *MT03*) developed the Turbulent Core model, based on the assumptions that the internal pressure is mostly non-thermal, in the form of turbulence and/or magnetic fields, and that the initial core is reasonably close to internal virial equilibrium, so that its structure can be approximated as a singular polytropic sphere. Also, approximate pressure equilibrium with the surrounding clump is assumed, which thus normalizes the size, density and velocity dispersion of a core of given mass to Σ_{cl} . *MT03* focused on the case in which $\rho \propto r^{-k_\rho}$ with $k_\rho = 1.5$, similar to observed values (§3.1); for this case, $\Sigma_c = 1.22\Sigma_{\text{cl}}$. For example, the core radius, given by eq. (1) with core properties in place of those of the clump, can be expressed in terms of core mass and clump surface density: $R_c = 0.074(M_{c,2}/\Sigma_{\text{cl}})^{1/2} \text{ pc}$.

The characteristic accretion rate in Core Accretion models is given by eq. (12). In the *Shu* (1977) model, based on collapse of a singular isothermal sphere, the actual accretion rate is $0.38\dot{m}_{\text{ff}}$. This result ignores the contraction needed to create the sphere. *Tan and McKee* (2004) argued (in the context of primordial star formation, but similar rea-

soning may apply locally) that it was more reasonable to include the formation phase of the collapsing cloud using one of *Hunter's* (1977) subsonic collapse solutions, which has an accretion rate 2.6 times larger and gives an accretion rate onto the star + disk system of $\dot{m}_{*d} \simeq \dot{m}_{\text{ff}}$. For collapse that begins from a marginally stable Bonnor-Ebert sphere, \dot{m}_{*d} is initially $\gg \dot{m}_{\text{ff}}$, but then falls to about the Shu rate. For the Turbulent Core model, the dependence of the accretion rate on $M\Sigma$ can be re-expressed in terms of the current value of the idealized collapsed-mass that has been supplied to the central disk in the zero-feedback limit, M_{*d} , (note, the actual protostar plus disk mass accretion rate is $\dot{m}_{*d} = \epsilon_{*d}\dot{M}_{*d}$ and the integrated protostar plus disk mass is $m_{*d} = \bar{\epsilon}_{*d}M_{*d}$) and Σ_{cl} . For $k_\rho = 1.5$ and allowing for the effects of magnetic fields (*MT03*), this gives

$$\dot{m}_{*d} = 1.37 \times 10^{-3} \epsilon_{*d} (M_{c,2} \Sigma_{\text{cl}})^{3/4} (M_{*d}/M_c)^{1/2} M_\odot \text{yr}^{-1}; \quad (14)$$

for $\epsilon_{*d} = 1$, this corresponds to $\dot{m}_{*d} = 0.64\dot{m}_{\text{ff}}$. If the disk mass is assumed to be a constant fraction, f_d , of the stellar mass, then the actual accretion rate to the protostar is $\dot{m}_* = (1/[1 + f_d])\dot{m}_{*d}$. A value of $f_d \simeq 1/3$, i.e., a relatively massive disk, is expected in models where angular momentum transport is due to moderately self-gravitating disk turbulence and larger-scale spiral density waves.

Two challenges faced by Core Accretion are: (1) What prevents a massive core, perhaps containing $\sim 10^2$ Jeans masses, fragmenting into a cluster of smaller stars? This will be addressed in §2.4. (2) Where are the accretion disks expected around forming single and binary massive stars? Disks have been discovered around some massive stars, but it has not been shown that they are ubiquitous (§4.2).

2.2.2. Competitive Accretion

Competitive Accretion (*Bonnell et al.*, 2001) involves protostars accreting ambient clump gas at a rate

$$\dot{m}_{*d} = \pi \rho_{\text{cl}} v_{\text{rel}}^2 r_{\text{acc}}^2, \quad (15)$$

where v_{rel} is the relative velocity of stars with respect to clump gas, ρ_{cl} is the local density, and r_{acc} is the accretion radius. Two limits for r_{acc} were proposed: (1) Gas-dominated regime (set by tidal radius): $r_{\text{acc}} \simeq r_{\text{tidal}} = 0.5[m_*/M_{\text{cl}}(R)]^{1/3}R$, where R is the distance of the star from the clump center; (2) star-dominated regime (set by Bondi-Hoyle accretion radius): $r_{\text{acc}} \simeq r_{\text{BH}} = 2Gm_*/(v_{\text{rel}}^2 + c_s^2)$. The star-dominated regime was suggested to be relevant for massive star formation—the stars destined to become massive being those that tend to settle to protocenter centers, where high ambient gas densities are maintained by global clump infall. The accretion is assumed to be terminated by stellar feedback or by fragmentation induced starvation (*Peters et al.*, 2010b).

In addition to forming massive stars, *Bonnell et al.* (2001; 2007) proposed Competitive Accretion is also responsible for building up the IMF for $m_* \gtrsim M_{\text{BE}}$. These studies have since been developed to incorporate additional

physics (see §2.5) and include comparisons to both the IMF and binary properties of the stellar systems (*Bate*, 2012).

Bonnell et al. (2004) tracked the gas that joined the massive stars in their simulation, showing it was initially widely distributed throughout the clump, so the final mass of the star did not depend on the initial core mass present when it first started forming. Studies of the gas cores seen in simulations exhibiting Competitive Accretion have been carried out by *Smith et al.* (2011, 2013), with non-spherical, filamentary morphologies being prevalent, along with total accretion being dominated by that accreted later from beyond the original core volume. Other predictions of the Competitive Accretion scenario are relatively small accretion disks, with chaotically varying orientations, which would also be reflected in protostellar outflow directions. Massive stars would always be observed to form at the center of a cluster in which the stellar mass was dominated by low-mass stars.

As Competitive Accretion is “clump-fed”, we express the average accretion rate of a star of final mass m_{*f} via

$$\begin{aligned} \langle \dot{m}_{*d} \rangle &= \epsilon_{\text{ff}} \dot{m}_{\text{ff}} m_{*f} / (\epsilon_{\text{cl}} M_{\text{cl}}) & (16) \\ &\rightarrow 1.46 \times 10^{-4} \epsilon_{\text{ff},0.1} \frac{m_{*f,50}}{\epsilon_{\text{cl},0.5}} \frac{\Sigma_{\text{cl}}^{3/4}}{M_{\text{cl},3}^{1/4}} M_\odot \text{yr}^{-1} \end{aligned}$$

(see also *Wang et al.*, 2010), where ϵ_{ff} is the star formation efficiency per free-fall time and ϵ_{cl} is the final star formation efficiency from the clump. *Krumholz and Tan* (2007) estimated $\epsilon_{\text{ff}} \simeq 0.04$ in the ONC. The average accretion rate ($4.6 \times 10^{-5} M_\odot \text{yr}^{-1}$) of the most massive star ($46.4 M_\odot$) in the *Wang et al.* (2010) simulation with outflow feedback ($\Sigma_{\text{cl}} = 0.08 \text{ g cm}^{-2}$, $M_{\text{cl}} = 1220 M_\odot$, $\epsilon_{\text{cl}} = 0.18$, $\epsilon_{\text{ff}} = 0.08$) agrees with eq. (16) to within 10%. This shows that a major difference of the Competitive Accretion model of massive star formation from Core Accretion is that its average accretion rate to the star is much smaller (cf., eq. 14).

This low rate of competitive accretion was noted before in the context of accretion from a turbulent medium with $\alpha_{\text{vir}} \sim 1$, as is observed in most star-forming regions (*Krumholz et al.*, 2005a). *Bonnell et al.* (2001) came to essentially the same conclusion by noting competitive accretion would not be fast enough to form massive stars, if stars were virialized in the cluster potential (i.e., high v_{rel}). They suggested efficient star formation ($\epsilon_{\text{ff}} \sim 1$) occurs in regions of global gravitational collapse with negligible random motions. *Wang et al.* (2010), by including the effects of protostellar outflows and moderately strong magnetic fields that slowed down star cluster formation, found massive star formation via competitive accretion occurred relatively slowly over about 1 Myr (eq. 16). Accretion to the clump center was fed by a network of dense filaments, even while the overall clump structure remained in quasi virial equilibrium. As discussed further in §2.5, these results may depend on the choice of initial conditions, such as the degree of magnetization and/or use of an initially smooth density field, which minimizes the role of turbulence.

Another challenge for Competitive Accretion is the effect of feedback. *Edgar and Clarke* (2004) noted radia-

tion pressure disrupts dusty Bondi-Hoyle accretion for protostellar masses $\gtrsim 10 M_{\odot}$. Protostellar outflows, such as those included by *Wang et al.* (2010), also impede local accretion to a star from some directions around the accretion radius. This issue is examined further in §2.4.

In sum, the key distinction between Competitive and Core Accretion is whether competitive, “clump-fed” accretion of gas onto stars, especially intermediate and massive stars, dominates over that present in the initial pre-stellar core (PSC). In Core Accretion, the PSC will likely gain some mass via accretion from the clump, but it will also lose mass due to feedback; the net result is that the mass of the PSC will be $\gtrsim m_{*f}$. In Competitive Accretion, the PSC mass is $\ll m_{*f}$. Of course, reality may be somewhere between these extremes, or might involve different aspects. We note that an observational test of this theoretical distinction requires that it be possible to identify PSCs that may themselves be turbulent. As discussed in §2.5, to date no simulations have been performed with self-consistent initial conditions and with the full range of feedback. Such simulations will be possible in the near future and should determine whether massive PSCs can form in such an environment, as required for Core Accretion models, or whether low/intermediate mass stars can accrete enough mass by tidally truncated Bondi accretion to grow into massive stars.

2.2.3. Protostellar Collisions

Bonnell et al. (1998) proposed massive stars may form (i.e., gain significant mass) via protostellar collisions, including those resulting from the hardening of binaries (*Bonnell and Bate*, 2005). This model was motivated by the perceived difficulty of accreting dusty gas onto massive protostars—merging protostars are optically thick and so unaffected by radiation pressure feedback. Note, such protostellar collisions are distinct from those inferred to be driven by binary stellar evolution (*Sana et al.*, 2012). Universal formation of massive stars via collisions would imply massive stars always form in clusters. Indeed, for collisional growth to be rapid compared to stellar evolution timescales requires cluster environments of extreme stellar densities, $\gtrsim 10^8 \text{ pc}^{-3}$ (i.e., $n_{\text{H}} \gtrsim 3 \times 10^9 \text{ cm}^{-3}$) (e.g., *Moeckel and Clarke*, 2011; *Baumgardt and Klessen*, 2011), never yet observed (Fig. 1). *Moeckel and Clarke* (2011) find that when collisions are efficient, they lead to runaway growth of one or two extreme objects, rather than smoothly filling the upper IMF. Thus collisional growth appears to be unimportant in typical massive star-forming environments.

2.3. Accretion Disks and Protostellar Evolution

In both Core and Competitive Accretion, the angular momentum of the gas is expected to be large enough that most accretion to the protostar proceeds via a disk. Here angular momentum is transferred outwards via viscous torques resulting from the magneto-rotational instability (MRI) or gravitational instability, which produces spiral arms and, if strong enough, fragmentation to form a binary or higher or-

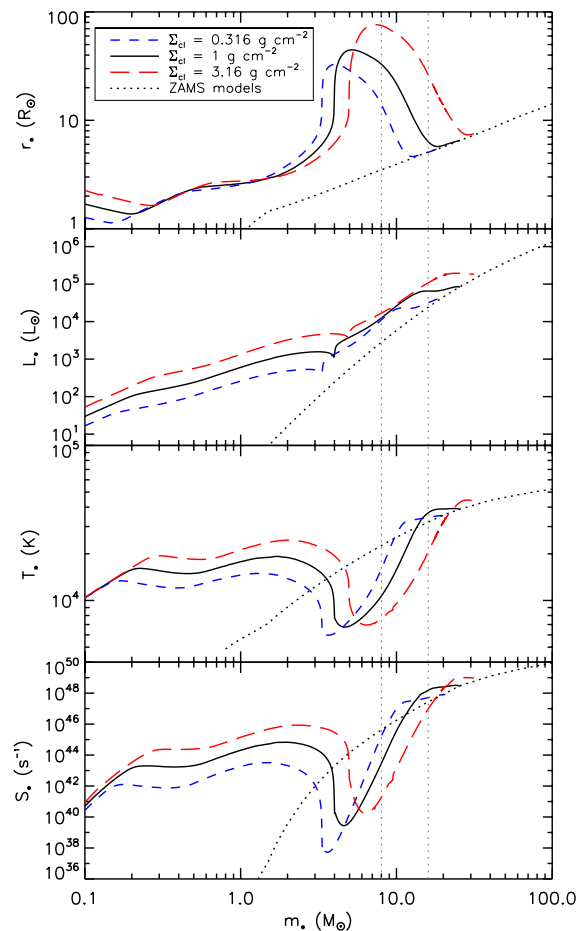


Fig. 2.— Evolution of a massive protostar forming from a $60 M_{\odot}$ core in $\Sigma_{\text{cl}} \simeq 0.3, 1, 3 \text{ g cm}^{-2}$ clumps. Top to bottom: radius, luminosity (including accretion), surface temperature and H-ionizing luminosity (*Zhang et al.*, 2014; see also *Hosokawa et al.*, 2010). Dotted lines show the zero age main sequence (ZAMS).

der multiple (*Kratter et al.*, 2010). For the Turbulent Core model, an upper limit for the size of the disk forming in a core of rotational energy $\beta_{\text{rot}} = E_{\text{rot}}/|E_{\text{grav}}|$ is evaluated by assuming conservation of angular momentum of gas streamlines inside the sonic point of the flow. Then the disk radius, r_d , is a fraction of the initial core size: for a $60 M_{\odot}$, $\beta_{\text{rot}} = 0.02$ core forming in a clump with $\Sigma_{\text{cl}} = 1 \text{ g cm}^{-2}$, we have $r_d = 57.4, 102 \text{ AU}$ when $m_* = 8, 16 M_{\odot}$ (*Zhang et al.*, 2014; see Figs. 2 & 3). However, magnetic braking of the accretion flow may make the disk much smaller (*Z.-Y. Li et al.*, this volume). Disks around massive protostars also arise in Competitive Accretion models (e.g., *Bate*, 2012), but are likely to be smaller than in Core Accretion models.

Angular momentum may also be transferred via torques associated with a large-scale magnetic field threading the disk that couples to a disk wind (*Blandford and Payne*, 1982; *Königl and Pudritz*, 2000). The final accretion to the protostar may be mediated by a strong stellar B -field, as proposed for X-wind models around low-mass protostars

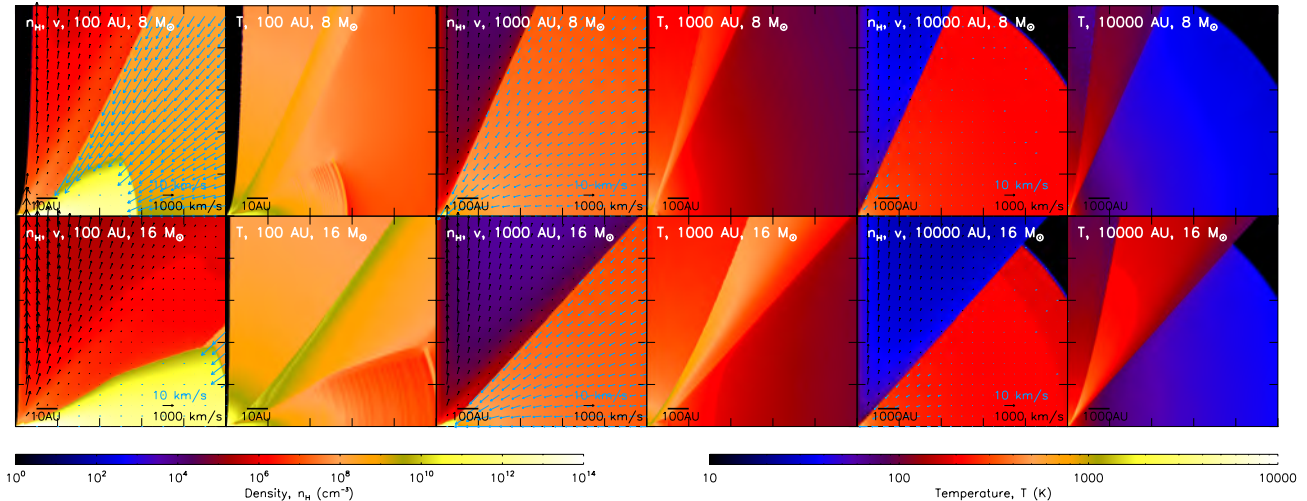


Fig. 3.— Density and temperature profiles for a massive protostellar core (Zhang *et al.*, 2014), when the central protostar (at bottom left of each panel) reaches $m_* = 8 M_\odot$ (top row) and $16 M_\odot$ (bottom row). The disk midplane coincides with the x-axis; the outflow/rotation axis with the y-axis. The core has initial mass $M_c = 60 M_\odot$ and rotational to gravitational energy ratio of $\beta_{\text{rot}} = 0.02$ and is embedded in a clump with mean surface density $\Sigma_{\text{cl}} = 1 \text{ g cm}^{-2}$. At each stage, three pairs of box sizes are shown (left to right, 100, 10^3 , 10^4 AU). Overlaid on density plots are blue/black arrows showing infall/outflow velocities (arrow length scale is 10/1000 km s^{-1} , respectively).

(Shu *et al.*, 2000). For massive stars, the required field strengths would need to be $\gtrsim \text{kG}$ (Rosen *et al.*, 2012). Or, the disk may continue all the way in to the protostellar surface, in which case one expects high (near break-up) initial rotation rates of massive stars. However, such high rates are typically not observed and the necessary spin down would require either stronger B -fields or longer disk lifetimes than those inferred from observations (Rosen *et al.*, 2012).

The evolution of the protostar depends on its rate of accretion of mass, energy and angular momentum from the disk. Since the dynamical time of the star is short compared to the growth time, this process is typically modeled as a sequence of equilibrium stellar structure calculations (e.g., Palla and Stahler, 1991; Hosokawa *et al.*, 2010; Kuiper and Yorke, 2013; Zhang *et al.*, 2014). Most models developed so far have been for non-rotating protostars (see Haemmerlé *et al.*, 2013 for an exception). A choice must also be made for the protostellar surface boundary condition: photospheric or non-photospheric. In the former, accreting material is able to radiate away its high internal energy that has just been produced in the accretion shock, while in the latter the gas is optically thick (i.e., the photosphere is at a larger radius than the protostellar surface). At a given mass, the protostar will respond to advecting more energy by having a larger size. If accretion proceeds through a disk, this is usually taken to imply photospheric boundary conditions (cf., Tan and McKee, 2004). In the calculation shown in Fig. 2, transition from quasi-spherical, non-photospheric accretion is made to photospheric at $m_* \lesssim 0.1 M_\odot$ based on an estimate of when outflows first affect the local environment. Subsequent evolution is influenced by D-burning,

“luminosity-wave” swelling and contraction to the zero age main sequence (ZAMS) once the protostar is older than its current Kelvin-Helmholtz time. This explains why protostars with higher accretion rates, i.e., in higher Σ_{cl} clumps, reach the ZAMS at higher masses. Protostars may still accrete along the ZAMS. The high temperatures and ionizing luminosities of this phase are a qualitative difference from lower-mass protostars, especially leading to ionization of the outflow cavity and eventually the core envelope (§2.4).

Radiative transfer (RT) calculations are needed to predict the multiwavelength appearance and total spectral energy distribution (SED) of the protostar (e.g., Robitaille *et al.*, 2006; Molinari *et al.*, 2008; Johnston *et al.*, 2011; Zhang and Tan, 2011; Zhang *et al.*, 2013a; 2014). The luminosity of the protostar and disk are reprocessed by the surrounding gas and dust in the disk, envelope and outflow cavity. Figure 3 shows example models of the density, velocity and temperature structure of a massive protostar forming inside a $60 M_\odot$ core embedded in a $\Sigma_{\text{cl}} = 1 \text{ g cm}^{-2}$ environment at two stages, when $m_* = 8$ and $16 M_\odot$, zooming from the inner 100 to 10^3 to 10^4 AU (Zhang *et al.*, 2014). One feature of these models is that they self-consistently include the evolution of the protostar from the initial starless core in a given clump environment, including rotating infall envelope, accretion disk and disk-wind-driven outflow cavities, that gradually open up as the wind momentum flux becomes more powerful (§2.4). These models are still highly idealized, being axisymmetric about a single protostar. A real source would most likely be embedded in a forming cluster that includes other protostars in the vicinity.

Similar continuum RT calculations have yet to be made

for Competitive Accretion. We anticipate they would show more disordered morphologies and have smaller masses and Σ s of gas in the close vicinity of the protostar than Core Accretion models, which may affect their SEDs at a given evolutionary stage, i.e., value of m_* . These potential SED differences are worth exploring, especially at the stages when ionization becomes important for creating hypercompact (HC) and ultracompact (UC) H II regions (§2.4).

2.4. Feedback Processes During Accretion

Massive protostars are much more luminous and hotter than low-mass protostars so, all else being equal, one expects radiative feedback (i.e., thermal heating, dissociation/ionization of hydrogen, radiation pressure on dust) to be more important. The same is true for mechanical feedback from stellar winds (i.e., those from the stellar surface) and protostellar outflows (magneto-centrifugally-driven flows powered by accretion). Alternatively, if massive stars tend to form in denser, more highly-pressurized environments, then feedback will have a harder time disrupting accretion. For Core Accretion models, a major goal of feedback studies is to estimate the star formation efficiency from a core of a given initial mass and density (or surrounding clump pressure). For both Core and Competitive Accretion, an important goal is to determine whether there are processes that lead to IMF truncation at some maximum mass. Feedback may also affect the ability of a core to fragment to form a binary and the efficiency of a clump to fragment into a cluster. Feedback also produces observational signatures, such as outflow cavities, H II regions and excitation of masers, that all serve as diagnostics of massive star formation. A general review of feedback is given by *Krumholz et al.* in this volume. Here we discuss processes directly relevant to massive star formation.

For massive stars to form from massive cores, a mechanism is needed to prevent the core from fragmenting. *Krumholz and McKee* (2008) suggested this may be due to radiative feedback from surrounding lower-mass protostars that have high accretion luminosities if they are forming in a high pressure clump. This model predicts a minimum Σ for clumps to form massive stars, $\Sigma_{\text{cl}} \gtrsim 1 \text{ g cm}^{-2}$. On the other hand, *Kunz and Mouschovias* (2009) and *Tan et al.* (2013b) invoked a non-feedback-related mechanism of magnetic field support to allow massive cores to resist fragmentation. This does not require a minimum Σ_{cl} threshold, but does require that there be relatively strong, $\sim \text{mG}$, B -fields in at least some parts of the clump, so that the core mass is set by the magnetic critical mass. Simulations confirm that magnetic fields can suppress fragmentation (§2.5). The observational evidence for a whether there is a Σ_{cl} threshold for massive star formation is discussed in §4.7.

Once a massive protostar starts forming, but before contraction to the ZAMS, the dominant feedback is expected to be due to protostellar outflows (see also §4.3). As a consequence of their extraction of angular momentum, these magneto-centrifugally-launched disk- and/or X-winds tend to have mass flow rates $\dot{m}_w = f_w \dot{m}_*$ with $f_w \sim 0.1 - 0.3$

and terminal velocities $v_w \sim v_K(r_0)$, where v_K is the Keplerian speed in the disk at the radius, r_0 , of the launching region. The total outflow momentum flux can be expressed as $\dot{p}_w = \dot{m}_w v_w = f_w \dot{m}_* v_w \equiv \phi_w \dot{m}_* v_K(r_*)$: *Najita and Shu* (1994) X-wind models have dimensionless parameter $\phi_w \simeq 0.6$. An implementation of the *Blandford and Payne* (1982) disk-wind model has $\phi_w \simeq 0.2$, relatively independent of m_* (*Zhang et al.*, 2013a). Outflows are predicted to be collimated with $dp_w/d\Omega = (p_w/4\pi)[\ln(2/\theta_0)(1+\theta_0^2-\mu^2)]^{-1}$ (*Matzner and McKee*, 1999), where $\mu = \cos\theta$, θ is the angle from outflow axis, and $\theta_0 \sim 10^{-2}$ is a small angle of the core of the outflow jet. *Matzner and McKee* (2000) found star formation efficiency from a core due to such outflow momentum feedback of $\bar{\epsilon}_{*d} \sim 0.5$. For the protostars in Fig. 2, $\bar{\epsilon}_{*d} \simeq 0.45, 0.57, 0.69$ for $\Sigma_{\text{cl}} = 0.3, 1, 3 \text{ g cm}^{-2}$, indicating protostellar outflow feedback may set a relatively constant formation efficiency from low to high mass cores.

The protostar’s luminosity heats its surroundings, mostly via absorption by dust, which at high densities ($n_{\text{H}} \gtrsim 10^5 \text{ cm}^{-3}$) is well-coupled thermally to the gas (*Urban et al.*, 2010). Dust is destroyed at $T \gtrsim 1500 \text{ K}$, i.e., at $\lesssim 10 \text{ AU}$ for models in Fig. 3. Hot core chemistry (§4.5) is initiated for temperatures $\gtrsim 100 \text{ K}$. Thermal heating reduces subsequent fragmentation in the disk (see §2.5).

As the protostar grows in mass and settles towards the main sequence, the temperature and H-ionizing luminosity begin to increase. The models in Fig. 3 have H-ionizing photon luminosities of $2.9 \times 10^{43} \text{ s}^{-1}$ and $1.6 \times 10^{48} \text{ s}^{-1}$ when $m_* = 8 M_{\odot}$ and $16 M_{\odot}$, respectively. A portion of the inner outflow cavity will begin to be ionized—an “outflow-confined” H II region (*Tan and McKee*, 2003). Inner, strongly-bound parts of the infall envelope that are unaffected by outflows could also confine the H II region (*Keto*, 2007). The H II region structure is detectable via radio continuum observations of thermal bremsstrahlung emission (§4.4). Its extent depends sensitively on the density and dust content of the gas. Feedback from the H II region is driven by its high temperature, $\sim 10^4 \text{ K}$, that sets up a pressure imbalance at the ionization front boundary with neutral gas. Since the MHD-outflow momentum flux is likely to dominate over the H II region thermal pressure, ionization feedback will only begin to be effective once the entire outflow cavity is ionized and ionization fronts start to erode the core infall envelope (cf., *Peters et al.*, 2011). Once the core envelope is mostly cleared, leaving equatorial accretion and a remnant accretion disk, the diffuse ionizing radiation field that is processed by the disk atmosphere can photoevaporate the disk (*Hollenbach et al.*, 1994). This process has been invoked by *McKee and Tan* (2008) to shut off accretion of the first stars around $\sim 100 - 200 M_{\odot}$ (see also *Hosokawa et al.*, 2011; *Tanaka et al.* 2013), but its role in present-day massive star formation is unclear, especially given the presence of dust that can absorb ionizing photons.

Radiation pressure acting on dust has long been regarded as a potential impediment to massive star formation (*Larson & Starrfield*, 1971; *Kahn*, 1974; *Wolfire and Cassinelli*, 1987). However, as long as the accretion flow remains opti-

cally thick, e.g., in a disk, then there does not seem to be any barrier to forming massive stars (Nakano, 1989; Jijina and Adams, 1996; Yorke and Sonnhalter, 2002; Krumholz et al., 2009; Kuiper et al., 2010a; 2011; Tanaka and Nakamoto, 2011). Outflows also reduce the ability of radiation pressure to terminate accretion, since they provide optically thin channels through which the radiation can escape (Krumholz et al., 2005b). This contributes to the “flashlight effect” (Yorke and Sonnhalter, 2002; Zhang et al., 2013a), leading to factors of several variation in the bolometric flux of a protostar depending on viewing angle. Numerical simulations of radiation pressure feedback are summarized in §2.5.

A potential major difference between Core and Competitive Accretion is their ability to operate in the presence of feedback. As discussed above, core accretion to a disk is quite effective at resisting feedback: gas comes together into a self-gravitating object before the onset of star formation. Competitive accretion of ambient gas from the clump may be more likely to be disrupted by feedback. Considering the main feedback mechanism for low-mass stars, we estimate the ram pressure associated with a MHD (X- or disk-) wind of mass-loss rate \dot{m}_w and velocity v_w as $P_w = \rho_w v_w^2 = f_\theta \dot{m}_w v_w / (4\pi r^2) = f_\theta \phi_w \dot{m}_* v_K(r_*) / (4\pi r^2)$, where $f_\theta \equiv 0.1 f_{\theta,0.1}$ is the factor by which the momentum flux of the wide-angle component of the wind is reduced from the isotropic average and where we have normalized, conservatively, to parameter values implied by disk-wind or X-wind models (e.g., the fiducial Matzner and McKee, 1999 distribution has a minimum $f_\theta \simeq 0.2$ at $\theta = 90^\circ$). Evaluating P_w at $r_{\text{BH}} = 2Gm_*/\sigma^2$ (appropriate for competitive accretion from a turbulent clump) around a protostar of current mass $m_* \equiv m_{*,1} M_\odot$, adopting accretion rates from eq.(16) and setting $r_* \equiv r_{*,3} 3R_\odot$ (Fig. 2), we find the condition for the clump mean pressure to overcome the ram pressure of the wind, $\bar{P}_{\text{cl}} > P_w(r_{\text{BH}})$:

$$\Sigma_{\text{cl}} > 11.7 \left(\frac{f_{\theta,0.1} \phi_{w,0.1} \alpha_{\text{vir}} \epsilon_{\text{ff},0.1}}{\phi_B \phi_{\text{geom}} \epsilon_{\text{cl},0.5}} \right)^4 \frac{M_{\text{cl},3}^3 m_{*,f,1}^4}{r_{*,3}^2 m_{*,1}^6} \text{g cm}^{-2} \quad (17)$$

Thus in most clumps shown in Fig. 1, \bar{P}_{cl} is too weak to confine gas inside the Bondi radius in the presence of such outflows. Note, here m_* is the mass scale at which feedback is being considered, while $m_{*,f}$ parameterizes the accretion rate needed to form a star of final mass $m_{*,f}$. Eq. (17) shows MHD-wind feedback generated by the accretion rates expected in Competitive Accretion severely impacts accretion over most of the Bondi-sphere, especially if the mass scale at which competitive accretion starts, following initial core accretion, is small ($m_* \sim 1 M_\odot$). We suggest simulations have so far not fully resolved the effects of MHD-wind feedback on competitive accretion and that this feedback may lead to a major reduction in its efficiency.

2.5. Results from Numerical Simulations

Numerical simulations have long been a major tool for investigating massive star formation. Today, the majority use either the Lagrangian technique smoothed particle hy-

drodynamics (SPH; e.g., Lucy, 1977) or the Eulerian technique adaptive mesh refinement (AMR; Berger and Olinger, 1984), both of which provide high dynamic range allowing collapse to be followed over orders of magnitude in length scale in general geometries. Both code types include self-gravity, hydrodynamics and sink particles to represent stars (e.g., Bate et al., 1995; Krumholz et al., 2004).

Probably the most significant advance in simulations since Protostars & Planets V has been addition of extra physical processes. For SPH, there are implementations of magnetohydrodynamics (Price and Monaghan, 2004), flux-limited diffusion (FLD) for RT of dust-reprocessed non-ionizing radiation (Whitehouse and Bate, 2004), and ray-tracing for ionizing RT (Dale et al., 2005; Bisbas et al., 2009), the latter specifically used to study massive star formation. AMR codes include an even broader range of physics, all of which has been brought to bear on massive star formation: MHD (e.g., Fryxell et al., 2000; Li et al., 2012a), FLD for non-ionizing radiation (Krumholz et al., 2007b; Commerçon et al., 2011b), ray-tracing for ionizing and (in restricted circumstances) non-ionizing radiation (Peters et al., 2010a), and protostellar outflows (Wang et al., 2010; Cunningham et al., 2011). More sophisticated RT schemes than pure FLD or ray-tracing are also available in some non-adaptive grid codes (e.g., Kuiper et al., 2010b).

While this is progress, a few caveats are in order. First, no code yet includes all of these physical processes: e.g., ORION includes MHD, dust-reprocessed radiation and outflows, but not ionizing radiation, while FLASH has MHD and ionizing radiation, but not outflows or dust-reprocessed radiation. Second, some physical processes have only been studied in isolation by a single code and their relative importance is unclear. Examples include imperfect thermal coupling between gas and dust (Urban et al., 2010), dust coagulation and drift relative to gas (Suttner et al., 1999), and ambipolar drift (Duffin and Pudritz, 2008).

Still, the advances in simulation technique have yielded some important general conclusions. First, concerning fragmentation, hydrodynamics-only simulations found that collapsing gas clouds invariably fragmented into stars with initial masses of $\sim 0.1 M_\odot$ (Bonnell et al., 2004; Dobbs et al., 2005), implying formation of massive stars would have to arise via subsequent accretion onto these fragments. However, Krumholz et al. (2007a, 2012) showed that adding non-ionizing, dust reprocessed radiative feedback suppresses this behavior, as the first few stars to form heat the gas around them via their accretion luminosities, raising the Jeans mass and preventing much fragmentation. Similarly, Hennebelle et al. (2011) showed that magnetic fields also inhibit fragmentation, and Commerçon et al. (2011a) and Myers et al. (2013; Fig. 4) have combined magnetic fields and radiation to show that the two together suppress fragmentation much more effectively than either one alone.

Second, massive star feedback is not very effective at halting accretion. Photoionization can remove lower density gas, but dense gas that is already collapsing onto a massive protostar is largely self-shielding and is not expelled by

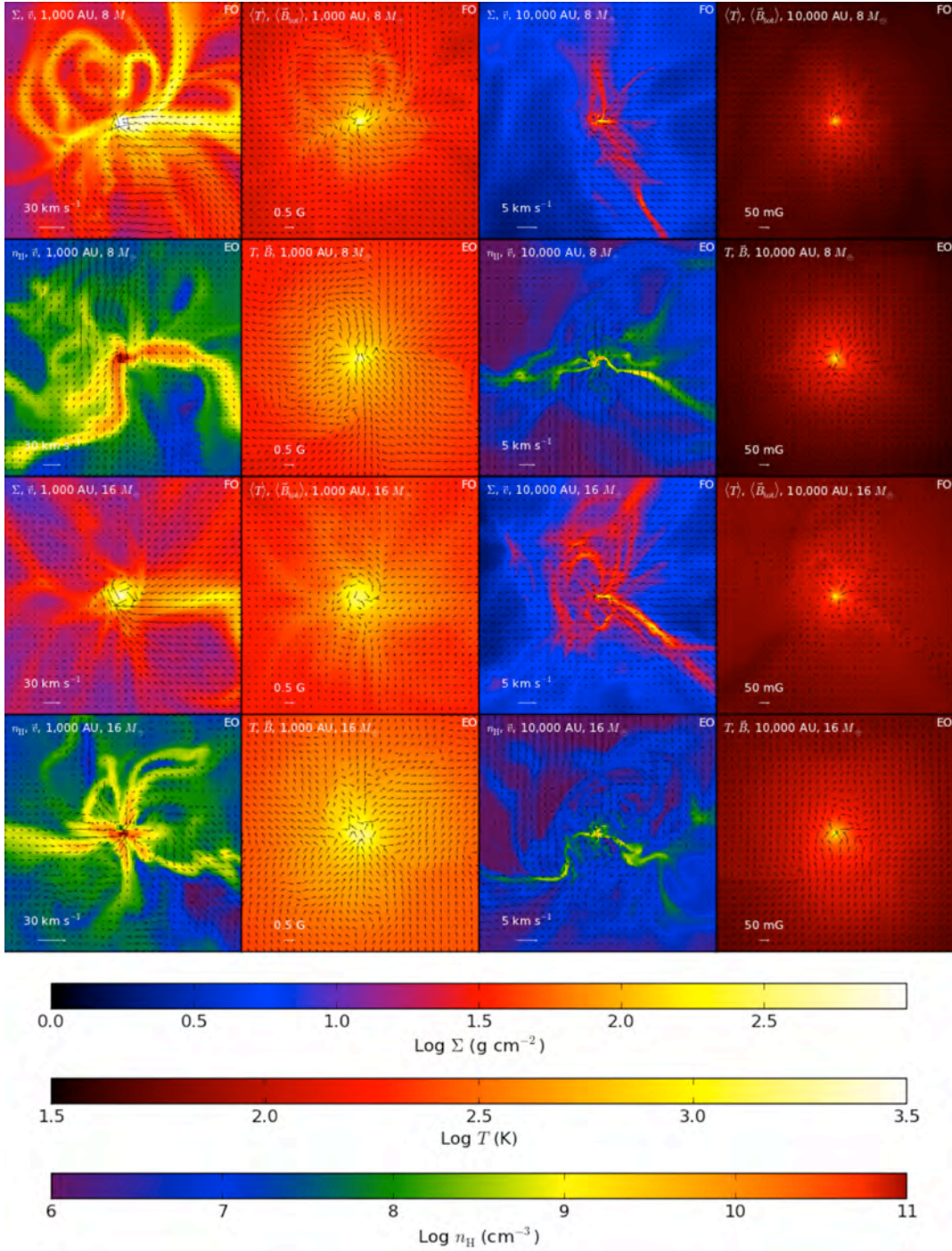


Fig. 4.— Simulation of massive star formation including MHD and radiation pressure feedback (Myers *et al.*, 2013) from an initial core with $M_c = 300 M_{\odot} \simeq 2M_{\Phi}$ (i.e., twice the magnetic critical mass), $\Sigma_c = 2 \text{ g cm}^{-2}$ and $\sigma = 2.3 \text{ km s}^{-1}$ (so that $\alpha_{\text{vir}} = 2.1$; turbulence decays, leading to global collapse). Protostellar outflow feedback (e.g., Wang *et al.*, 2010; Cunningham *et al.*, 2011) is not included. The top row shows a face-on (FO) view of the accretion disk centered on the protostar when it has a mass of $8 M_{\odot}$: from left to right are: mass surface density, Σ , and mean velocity, $\langle v \rangle$, (arrows) in a 10^3 AU box; mass-weighted temperature, $\langle T \rangle$, and total magnetic field strength, $\langle B_{\text{tot}} \rangle$, (arrows) in a 10^3 AU box; then the same two figures but for a 10^4 AU box. The second row shows edge-on (EO) views of this structure, with slices in a plane containing the protostar of, from left to right: H number density, n_{H} and velocity, v , (arrows) of a 10^3 AU square; temperature, T , and in-plane component of magnetic field, B , (arrows) of a 10^3 AU square; then the same two figures but for a 10^4 AU square. The third row repeats the first row, but now for a $16 M_{\odot}$ protostar, and the fourth row repeats the second row for this protostar. With an initially turbulent core, the accretion flow is relatively disordered (cf., Fig. 3).

ionizing radiation (Dale et al., 2005; Peters et al., 2010a; b; 2011). As for radiation pressure, 2D simulations with limited resolution (~ 100 AU) generally found that it could reverse accretion, thus limiting final stellar masses (Yorke and Sonnhalter, 2002). However, higher resolution 2D and 3D simulations find that radiation pressure does not halt accretion since, in optically thick flows, the gas is capable of reshaping the radiation field and beaming it away from the bulk of the incoming matter. This beaming can be provided by radiation Rayleigh-Taylor fingers (e.g., Krumholz et al., 2009; Jiang et al., 2013; cf., Kuiper et al., 2012), by an optically thick disk (Kuiper et al., 2010a, 2011; Kuiper and Yorke, 2013), or by an outflow cavity (Krumholz et al., 2005b; Cunningham et al., 2011).

While there is general agreement on the two points above, simulations have yet to settle the question of whether stars form primarily via Competitive or Core Accretion, or some hybrid of the two. Resolving this requires simulations large enough to form an entire star cluster, rather than focusing on a single massive star. Bonnell et al. (2004) and Smith et al. (2009) tracked the mass that eventually ends up in massive stars in their simulations of cluster formation, concluding that it is drawn from a ~ 1 pc cluster-sized region rather than a single well-defined ~ 0.1 pc core, and that there are no massive bound structures present. However, these simulations lacked radiative feedback or B -fields, and thus likely suffer from over-fragmentation. Wang et al. (2010) performed simulations including outflows and magnetic fields. They found the most massive star in their simulations ultimately draws its mass from a ~ 1 pc-sized reservoir comparable to the size of its parent cluster, consistent with Competitive Accretion, but that the flow on large scales is mediated by outflows, preventing onset of rapid global collapse. As described in §2.2.2, the average accretion rate to the massive star is relatively low in this simulation compared to the expectations of Core Accretion, which may be possible to test observationally (§4). As discussed in §2.4, outflow feedback on the scale of the Bondi accretion radius may be important in further limiting the rate of competitive accretion and so far has not been well resolved.

Peters et al. (2010a; b) simulated massive cluster formation with direct (i.e., not dust-reprocessed) radiation and B -fields, starting from smooth, spherical, slowly-rotating initial conditions. They found massive stars draw mass from large but gravitationally-bound regions, but that the mass flow onto these stars is ultimately limited by fragmentation of the accreting gas into smaller stars. Girichidis et al. (2012) extended this result to more general geometries. Krumholz et al. (2012) conducted simulations of cluster formation including radiation and starting from an initial condition of fully-developed turbulence. They found massive stars do form in identifiable massive cores, with several tens of solar masses within ~ 0.01 pc. Core mass is not conserved in a Lagrangian sense, as gas flows in or out, but they are nonetheless definable objects in an Eulerian sense.

These contradictory results likely have several origins. One is initial conditions (e.g., Girichidis et al., 2012).

Those lacking any density structure and promptly undergoing global collapse (e.g., Bonnell et al., 2004) tend to find there are no bound, massive structures that can be identified as the progenitors of massive stars, while those either beginning from saturated turbulence (e.g., Krumholz et al., 2012) or self-consistently producing it via feedback (e.g., Wang et al., 2010) do contain structures identifiable as massive cores. Another issue is the different range of included physical mechanisms, with none of the published cluster simulations combining dust-reprocessed radiation and magnetic fields—shown to be so effective at suppressing fragmentation on smaller scales. A final issue may simply be one of interpretation, with SPH codes tending to focus on the Lagrangian question of where the individual mass elements that make up a massive star originate, while Eulerian codes focus on the presence of structures at a particular point in space regardless of the paths of individual fluid elements.

3. OBSERVATIONS OF INITIAL CONDITIONS

3.1. Physical Properties of Starless Cores & Clumps

Initial conditions in Core Accretion models are massive starless cores, with $\Sigma \sim 1 \text{ g cm}^{-2}$, similar to the Σ s of their natal clump. For Competitive Accretion, massive stars are expected to form near the centers of the densest clumps. Thus to test these scenarios, methods are needed to study high Σ and volume density ($n_{\text{H}} \sim 10^6 \text{ cm}^{-3}$), compact ($r_c \sim 0.1$ pc, i.e., $7''$ at 3 kpc) and potentially very cold ($T \sim 10$ K) structures. Recently, many studies of initial conditions have focussed on Infrared Dark Clouds (IRDCs): regions with such high Σ that they appear dark at MIR ($\sim 10 \mu\text{m}$) and even up to FIR ($\sim 100 \mu\text{m}$) wavelengths. Indeed, selection of cores that may be starless often involves checking for the absence of a source at 24 or 70 μm .

3.1.1. Mass Surface Densities, Masses & Temperatures

One can probe Σ structures via MIR extinction mapping of IRDCs, using diffuse Galactic background emission from warm dust. *Spitzer* IRAC (e.g., GLIMPSE; Churchwell et al., 2009) 8 μm images resolve down to $2''$ and can probe to $\Sigma \sim 0.5 \text{ g cm}^{-2}$ (e.g., Butler and Tan, 2009; 2012 [BT12]; Peretto and Fuller, 2009; Ragan et al., 2009). The method depends on the 8 μm opacity per unit total mass, $\kappa_{8\mu\text{m}}$ (BT12 use $7.5 \text{ cm}^2 \text{ g}^{-1}$ based on the moderately coagulated thin ice mantle dust model of Ossenkopf and Henning, 1994), but is independent of dust temperature, T_d . Allowance is needed for foreground emission, best measured by finding “saturated” intensities towards independent, optically thick cores (BT12). Only differences in Σ relative to local surroundings are probed, so the method is insensitive to low- Σ IRDC environs. This limitation is addressed by combining NIR & MIR extinction maps (Kainulainen and Tan, 2013). Even with careful foreground treatment, there are $\sim 30\%$ uncertainties in κ and thus Σ , and, adopting 20% kinematic distance uncertainties, a 50% uncertainty in mass. Ten IRDCs studied in this way are shown in Fig. 1.

The high resolution Σ maps derived from *Spitzer* images

allow measurement of core and clump structure. Parameterizing density structure as $\rho \propto r^{-k_\rho}$ and looking at 42 peaks in their Σ maps, *BT12* found $k_\rho \simeq 1.1$ for “clumps” (based on total Σ profile) and $k_\rho \simeq 1.6$ for “cores” (based on Σ profile after clump envelope subtraction). These objects, showing total Σ , are also plotted in Fig. 1. A Σ map of one of these core/clumps is shown in Fig. 5. *Tan et al.* (2013b) used the fact that some of these cores are opaque at 70 μm to constrain $T_d \lesssim 13$ K. *Ragan et al.* (2009) measured an IRDC core/clump mass function, $dN/dM \propto M^{-\alpha_{\text{cl}}}$ with $\alpha_{\text{cl}} \simeq 1.76 \pm 0.05$ from 30 to 3000 M_\odot , somewhat shallower than that of the Salpeter stellar IMF ($\alpha_* \simeq 2.35$).

The Σ of these clouds can also be probed by the intensity, S_ν/Ω , of FIR/mm dust emission, requiring T_d and κ_ν . For optically thin RT and black body emission, $\Sigma = 4.35 \times 10^{-3} ([S_\nu/\Omega]/[\text{MJy/sr}]) \kappa_{\nu,0.01}^{-1} \lambda_{1.2}^3 [\exp(0.799 T_{d,15}^{-1} \lambda_{1.2}^{-1}) - 1] \text{ g cm}^{-2}$, where $\kappa_{\nu,0.01} \equiv \kappa_\nu/[0.01 \text{ cm}^2/\text{g}]^{-1}$, $\lambda_{1.2} \equiv \lambda/1.2 \text{ mm}$ and $T_{d,15} \equiv T_d/15 \text{ K}$. A common choice of κ_ν is again that predicted by the moderately coagulated thin ice mantle dust model of *Ossenkopf and Henning* (1994), with opacity per unit dust mass of $\kappa_{1.2\text{mm},d} = 1.056 \text{ cm}^2 \text{ g}^{-1}$. A gas-to-refractory-component-dust-mass ratio of 141 is estimated by *Draine* (2011) so $\kappa_{1.2\text{mm}} = 7.44 \times 10^{-3} \text{ cm}^2 \text{ g}^{-1}$. Uncertainties in κ_ν and T_d now contribute to Σ : e.g., *Tan et al.* (2013b) adopt κ uncertainties of 30% and $T_d = 10 \pm 3$ K, leading to factor ~ 2 uncertainties in 1.3 mm-derived Σ s. *Rathborne et al.* (2006) studied 1.2 mm emission at 11'' resolution in 38 IRDCs finding core/clumps with ~ 10 to $10^4 M_\odot$ (for $T_d = 15$ K). In their sample of 140 sources they found $dN/dM \propto M^{-\alpha_{\text{cl}}}$, with $\alpha_{\text{cl}} \simeq 2.1 \pm 0.4$.

Herschel observations of dust emission at 70 to 500 μm allow simultaneous measurement of T_d and Σ at ~ 20 – $30''$ resolution and numerous studies have been made of IRDCs (e.g., *Peretto et al.*, 2010; *Henning et al.*, 2010; *Beuther et al.*, 2010a; *Battersby et al.*, 2011; *Ragan et al.*, 2012). For MIR-dark regions, *Battersby et al.* (2011) derived a median $\Sigma \simeq 0.2 \text{ g cm}^{-2}$, but with some values extending to $\sim 5 \text{ g cm}^{-2}$. The median T_d of regions with $\Sigma \gtrsim 0.4 \text{ g cm}^{-2}$ was 19 K, but the high- Σ tail had $T_d \sim 10$ K.

Interferometric studies have probed mm dust emission at higher resolution. “Clumps” are often seen to contain substructure, i.e., a population of “cores”. CMF measurements have been attempted: e.g., *Beuther and Schilke* (2004; see also *Rodón et al.*, 2012) observed IRAS 19410+2336, finding $\alpha_c = 2.5$ from $M_c \sim 1.7$ to $25 M_\odot$ (but with few massive cores). While the similarity of CMF and IMF shapes is intriguing, there are caveats, e.g., whether cores are resolved; whether they are PSCs rather than non-star-forming overdensities or already star-forming cores; the possibility of mass-dependent lifetimes of PSCs (*Clark et al.*, 2007); and binary/multiple star formation from PSCs.

Some massive ($\sim 60 M_\odot$) cores, e.g., IRDC G28.34+0.06 P1 (*Zhang et al.*, 2009), Cygnus X N63 (*Bontemps et al.*, 2010; note recent detection of a bipolar outflow indicates a protostar is forming in this source, *Duarte-Cabral et al.*, 2013) and IRDC C1-S (*Tan et al.*, 2013b) (Figs. 1 & 5),

have apparently monolithic, centrally-concentrated structures with little substructure, even though containing many (~ 100) Jeans masses. This suggests fragmentation is being inhibited by a nonthermal mechanism, i.e., magnetic fields. *Tan et al.* (2013b) estimate ~ 1 mG field strengths are needed for the mass of C1-S to be set by its magnetic critical mass, given its density of $\bar{n}_\text{H} \simeq 6 \times 10^5 \text{ cm}^{-3}$.

Many molecular lines have been observed from IRDCs. Using integrated molecular line intensities to derive Σ is possible in theory, but common species like CO are frozen-out from the gas phase (see below), and other species still present have uncertain and likely spatially varying abundances. Nevertheless, if the astrochemistry is understood, then species that are expected to become relatively abundant in the cold, dense conditions of starless cores, such as deuterated N-bearing molecules (§3.2), can be used to identify PSCs, distinguishing them from the surrounding clump.

IRDC gas temperatures of 10–20 K have been derived from NH_3 inversion transitions (e.g., *Pillai et al.*, 2006; *Wang et al.*, 2008; *Sakai et al.*, 2008; *Chira et al.*, 2013).

3.1.2. Magnetic Fields

Polarization of dust continuum emission is thought to arise from alignment of non-spherical grains with B -fields and is thus a potential probe of plane-of-sky projected field morphology and, with greater uncertainty, field strength. The correlated orientation of polarization vectors with the orientations of filaments, together with the correlated orientations of polarization vectors of dense cores with their lower density surroundings (*H. Li et al.*, this volume) suggests B -fields play some role in the formation of dense cores. However, these polarization results are typically for relatively nearby molecular clouds, such as Taurus, Pipe Nebula and Orion, and only a few, lower-resolution studies have been reported for IRDCs (*Mathews et al.*, 2009).

Line-of-sight B -field strengths can be derived from Zeeman splitting of lines from molecules with an unpaired electron, such as OH, which probes lower-density envelopes, and CN, which traces denser gas. Unfortunately, measurement of Zeeman splitting in CN is very challenging observationally, requiring bright lines, and the reported measurements in massive star-forming regions are all towards already star-forming cores (§4). From the results of *Falgarone et al.* (2008) as summarized by *Crutcher* (2012), at densities $n_\text{H} \gtrsim 300 \text{ cm}^{-3}$, $B_{\text{max}} \simeq 0.44 (n_\text{H}/10^5 \text{ cm}^{-3})^{0.65} \text{ mG}$, with a distribution of B flat between 0 and B_{max} . Such field strengths, if present in massive starless cores like C1-S (Fig. 5), could support them against rapid free-fall collapse and fragmentation.

3.1.3. Kinematics and Dynamics

Measurement of cloud kinematics requires molecular line tracers, but again one faces the problem of being sure which parts of the cloud along the line of sight are being probed by a given tracer. The kinematics of ionized and neutral species can differ due to magnetic fields (*Houde et*

al., 2009). The spectra of molecular tracers of IRDCs, such as ^{13}CO , C^{18}O , N_2H^+ , NH_3 , HCN , HCO^+ , CCS , show line widths $\sim 0.5 - 2 \text{ km s}^{-1}$, i.e., consistent with varying degrees of supersonic turbulence (e.g., Wang et al., 2008; Sakai et al., 2008; Fontani et al., 2011). In studying the kinematics of IRDC G035.3900.33, Henshaw et al. (2013) have shown it breaks up into a few distinct filamentary components separated by up to a few kms^{-1} , and it is speculated these may be in the process of merging. Such a scenario may be consistent with the detection of widespread ($> \text{pc}$ -scale) SiO emission, a shock tracer, by Jiménez-Serra et al. (2010) along this IRDC. However, in general it is difficult to be certain about flow geometries from only line of sight velocity information. While infall/converging flow signatures have been claimed via inverse P-Cygni profiles in star-forming cores and clumps (§4), there are few such claims in starless objects (Beuther et al., 2013a). The L1544 PSC has $\sim 8 M_\odot$ and an infall speed of $\simeq 0.1 \text{ km s}^{-1}$ on scales of 10^3 AU —subsonic and $\ll v_{\text{ff}}$ (Keto and Caselli, 2010).

Given a measurement of cloud velocity dispersion, σ , the extent to which it is virialized can be assessed, but with the caveat that the amount of B -field support is typically unknown. Comparing ^{13}CO -derived σ s with MIR+NIR extinction masses, Kainulainen and Tan (2013) found $\bar{\alpha}_{\text{vir}} = 1.9$. Hernandez et al. (2012) compared MIR+NIR extinction masses with C^{18}O -derived σ s and surface pressures in strips across IRDC G035.3900.33, finding results consistent with virial equilibrium (Fiege and Pudritz, 2000).

For starless cores, Pillai et al. (2011) studied the dynamics of cold cores near UC H II regions using NH_2D -derived σ and 3.5 mm emission to measure mass, finding $\bar{\alpha}_{\text{vir}} \sim 0.3$. Tan et al. (2013b) measured mass and Σ from both MIR+NIR extinction and mm dust emission to compare predictions of the Turbulent Core Accretion model (including surface pressure confinement and Alfvén Mach number $\mathcal{M}_A = 1$ magnetic support) with observed σ , derived from N_2D^+ . In six cores they found a mean ratio of observed to predicted velocity dispersions of 0.81 ± 0.13 . However, for the massive monolithic core C1-S they found a ratio of 0.48 ± 0.17 , which at face value implies sub-virial conditions. However, virial equilibrium could apply if the magnetic fields were stronger so that $\mathcal{M}_A \simeq 0.3$ rather than 1, requiring $B \simeq 1.0 \text{ mG}$. Sánchez-Monge et al. (2013c) used NH_3 -derived mass and σ to find $\alpha_{\text{vir}} \sim 10$ for several tens of mostly low-mass starless cores, which would suggest they are unbound. However, they also found a linear correlation of M with virial mass $M_{\text{vir}} \equiv \alpha_{\text{vir}} M$, only expected if cores are self-gravitating, so further investigation of the accuracy of the absolute values of α_{vir} is needed.

3.2. Chemical Properties of Starless Cores & Clumps

IRDC chemical properties resemble those of low-mass dense cores (e.g., Vasyunina et al., 2012; Miettinen et al., 2011; Sanhueza et al., 2013), with widespread emission of NH_3 and N_2H^+ (e.g., Zhang et al., 2009; Henshaw et al., 2013). In the Nobeyama survey of Sakai et al. (2008),

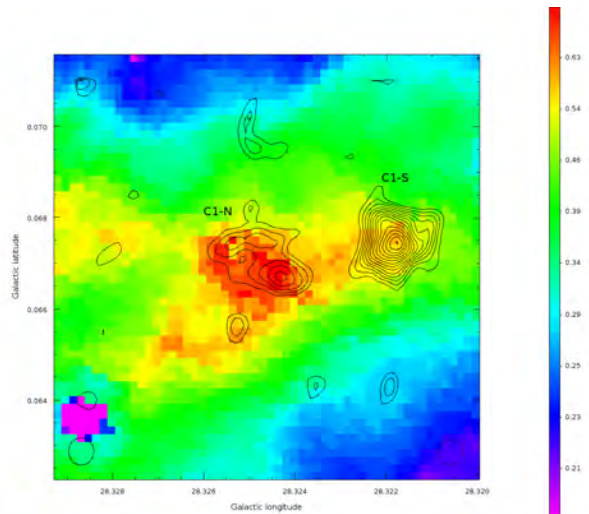


Fig. 5.— Candidate massive starless cores, C1-S & C1-N, traced by $\text{N}_2\text{D}^+(3-2)$ (contours), observed by ALMA (Tan et al., 2013b). Background shows MIR Σ map (g cm^{-2}). C1-S has $\sim 60 M_\odot$. The high value of $[\text{N}_2\text{D}^+]/[\text{N}_2\text{H}^+] \sim 0.1$ (Kong et al., in prep.) is a chemical indicator that C1-S is starless.

no CCS was detected, suggesting the gas is chemically evolved, i.e., atomic carbon is mostly locked into CO.

3.2.1. CO Freeze-Out

CO is expected to freeze-out from the gas phase onto dust grains when $T_d \lesssim 20 \text{ K}$ (e.g., Caselli et al., 1999). The CO depletion factor, $f_D(\text{CO})$, is defined as the ratio of the expected CO column density given a measured Σ (assuming standard gas phase abundances, e.g., $n_{\text{CO}}/n_{\text{H}_2} = 2 \times 10^{-4}$, Lacy et al., 1994) to the observed CO column density. Miettinen et al. (2011) compared CO(1-0) & (2-1) observations with Σ derived from FIR/mm emission finding no evidence for depletion. Hernandez et al. (2012) compared NIR & MIR-extinction-derived Σ with $\text{C}^{18}\text{O}(2-1)$ & (1-0) to map f_D in IRDC G035.39-00.33, finding widespread depletion with $f_D \sim 3$. Fontani et al. (2012) compared $\text{C}^{18}\text{O}(3-2)$ with FIR/mm-derived Σ in 21 IRDCs and found $\bar{f}_D \sim 30$, perhaps due to CO(3-2) tracing higher density (shorter depletion timescale) regions. On the other hand, Zhang et al. (2009) found $f_D \sim 10^2 - 10^3$ in IRDC G28.34+0.06 P1 & P2 by comparing $\text{C}^{18}\text{O}(2-1)$ to Σ from FIR/mm emission.

3.2.2. Deuteration

Freeze-out of CO and other neutrals boosts the abundance of (*ortho*-) H_2D^+ and thus the deuterium fractionation of other species left in the gas phase (Dalgarno and Lepp, 1984). Low-mass starless cores on the verge of star formation, i.e., PSCs, show an increase in $D_{\text{frac}}(\text{N}_2\text{H}^+) \equiv N(\text{N}_2\text{D}^+)/N(\text{N}_2\text{H}^+) \gtrsim 0.1$ (Crapsi et al., 2005). High (*ortho*-) H_2D^+ abundances are also seen (Caselli et al., 2008). In the protostellar phase, $D_{\text{frac}}(\text{N}_2\text{H}^+) & N(\text{H}_2\text{D}^+)$ decrease as the core envelope is heated (Emprechtinger et al., 2009; Ceccarelli et al., this volume).

To see if these results apply to the high-mass regime, Fontani et al. (2011) selected core/clumps, both starless and those associated with later stages of massive star formation, finding: (1) the average $D_{\text{frac}}(\text{N}_2\text{H}^+)$ in massive starless core/clumps located in quiescent environments tends to be as large as in low-mass PSCs (~ 0.2); (2) the abundance of N_2D^+ decreases in core/clumps that either harbor protostars or are starless but externally heated and/or shocked (see also Chen et al., 2011; Miettinen et al., 2011).

HCO^+ also becomes highly deuterated, but as CO freezes-out, formation rates of both HCO^+ and DCO^+ drop, so DCO^+ is not such a good tracer of PSCs as N_2D^+ . Deuteration of NH_3 is also high ($\gtrsim 0.1$) in starless regions of IRDCs, but, in contrast to N_2D^+ , can remain high in the protostellar phase (e.g., Pillai et al., 2011), perhaps since NH_2D & NH_3 also form in grains mantles, unlike N_2H^+ & N_2D^+ , so abundant NH_2D can result from mantle evaporation. DNC/HNC are different, with smaller $D_{\text{frac}}(\text{HNC})$ in colder, earlier-stage cores (Sakai et al., 2012).

3.2.3. Ionization Fraction

The ionization fraction, x_e , helps set the ambipolar diffusion timescale, t_{ad} , and thus perhaps the rate of PSC contraction. Observations of the abundance of molecular ions like H^{13}CO^+ , DCO^+ , N_2H^+ & N_2D^+ can be used to estimate x_e (Dalgarno 2006). Caselli et al. (2002) measured $x_e \sim 10^{-9}$ in the central regions of PSC L1544, implying $t_{\text{ad}} \simeq t_{\text{ff}}$. In massive starless cores, Chen et al. (2011) and Miettinen et al. (2011) found $x_e \sim 10^{-8} - 10^{-7}$, implying either larger cosmic-ray ionization rates or lower densities than in L1544. However, accurate estimates of x_e require detailed chemical modeling, currently lacking in the above studies, as well as knowledge of core structure—typically not well constrained. Core B -fields can also affect low-energy cosmic ray penetration, potentially causing variation in cosmic-ray ionization rate (Padovani and Galli, 2011).

3.3. Effect of Cluster Environment

The cluster environment may influence the physical and chemical properties of PSCs due to, e.g., warmer temperatures, enhanced turbulence, and (proto-)stellar interactions. Surveys of cores in cluster regions have started to investigate this issue, but have so far mostly targeted low-mass star-forming regions, like Perseus (e.g., Foster et al., 2009). These studies find cores have higher kinetic temperatures (~ 15 K) than isolated low-mass cores (~ 10 K). In spite of turbulent environments, cores have mostly thermal line widths.

Studies of proto-clusters containing an intermediate- or high-mass forming star (e.g., IRAS 05345+3157, Fontani et al., 2008; G28.34+0.06, Wang et al., 2008; W43, Beuther et al., 2012) have shown starless cores can have supersonic internal motions and $D_{\text{frac}}(\text{NH}_3, \text{N}_2\text{H}^+)$ values similar to low-mass star-forming regions. Sánchez-Monge et al. (2013c) analyzed VLA NH_3 data of 15 intermediate-/high-mass star-forming regions, finding 73 cores, classi-

fied as quiescent starless, perturbed starless or protostellar. The quiescent starless cores have smaller line widths and gas temperatures (1.0 km s^{-1} ; 16 K), than perturbed starless (1.4 km s^{-1} ; 19 K) and protostellar (1.8 km s^{-1} ; 21 K) cores. Still, even the most quiescent starless cores possess significant non-thermal components, contrary to the cores in low-mass star-forming regions. A correlation between core temperature and incident flux from the most massive star in the cluster was seen. These findings suggest the initial conditions of star formation vary depending on the cluster environment and/or proximity of massive stars.

3.4. Implications for Theoretical Models

The observed properties of PSCs, including their dependence on environment, constrain theoretical models of (massive) star formation. E.g., the massive ($\sim 60 M_{\odot}$), cold ($T_d \sim 10$ K), highly deuterated, monolithic starless core shown in Fig. 5 contains many Jeans masses, has modestly supersonic line widths, and requires relatively strong, $\sim \text{mG}$ magnetic fields if it is in virial equilibrium. More generally, the apparently continuous, power-law distribution of the shape of the low- to high-mass starless CMF implies fragmentation of dense molecular gas helps to shape the eventual stellar IMF. Improved observations of the PSC mass function (e.g., as traced by cores showing high deuteration of N_2H^+) are needed to help clarify this connection.

4. OBSERVATIONS OF THE ACCRETION PHASE

4.1. Clump and Core Infall Envelopes

Infall motions can be inferred from spectral lines showing an inverse P-Cygni profile. This results from optically thick line emission from a collapsing cloud with a relatively smooth density distribution and centrally-peaked excitation temperature. The profile shows emission on the blue-shifted side of line center (from gas approaching us on the cloud's far side) and self-absorption at line center and on the red-shifted side. Detection of a symmetric optically thin line profile from a rarer isotopologue helps confirm infall is being seen, rather than just independent velocity components.

Infall to low-mass protostars is seen via spectral lines tracing densities above $\sim 10^4 \text{ cm}^{-3}$ showing such inverse P-Cygni profiles (e.g., Mardones et al., 1997). Infall in high-mass protostellar cores is more difficult to find, given their typically larger distances and more crowded environments. It can also be difficult to distinguish core from clump infall. Single-dish observations of HCN, CS, HCO^+ , CO, & isotopologues (e.g., Wu and Evans, 2003; Wu et al. 2005b; Fuller et al., 2005; Barnes et al. 2010; Chen et al., 2010; López-Sepulcre et al., 2010; Schneider et al., 2010; Klaassen et al., 2012; Peretto et al., 2013) reveal evidence of infall on scales ~ 1 pc, likely relevant to the clump/protocluster. Derived infall velocities and rates range from $\sim 0.2 - 1 \text{ km s}^{-1}$ and $\sim 10^{-4} - 10^{-1} M_{\odot} \text{ yr}^{-1}$. However, these rates are very uncertain. López-Sepulcre et al. (2010) suggest they may be upper limits as the method

assumes most clump mass is infalling, whereas the self-absorbing region may be only a lower-density outer layer.

Clump infall times, $t_{\text{infall}} \equiv M_{\text{cl}}/\dot{M}_{\text{infall}}$ can be compared to t_{ff} . E.g., *Barnes et al.* (2010) measured $\dot{M}_{\text{infall}} \sim 3 \times 10^{-2} M_{\odot} \text{ yr}^{-1}$ in G286.21+0.17, with $M_{\text{cl}} \sim 10^4 M_{\odot}$ and $R_{\text{cl}} \simeq 0.45$ pc (Fig. 1). Thus $t_{\text{infall}}/t_{\text{ff}} \simeq 3.3 \times 10^5 \text{ yr}/5.0 \times 10^4 \text{ yr} = 6.7$. Note, this clump has the largest infall rate out of ~ 300 surveyed by *Barnes et al.* (2011). Similar results hold for the $\sim 10^3 M_{\odot}$ clumps NGC 2264 IRS 1 & 2 (*Williams and Garland, 2002*) with $t_{\text{infall}}/t_{\text{ff}} = 14, 8.8$, respectively. For the central region of SDC335 studied by *Peretto et al.* (2013), with $M_{\text{cl}} = 2600 M_{\odot}$, $R_{\text{cl}} = 0.6$ pc and $\dot{M}_{\text{infall}} = 2.5 \times 10^{-3} M_{\odot} \text{ yr}^{-1}$ (including boosting factor of 3.6 to account for accretion outside observed filaments), then $t_{\text{infall}}/t_{\text{ff}} = 7.0$. This suggests clump/cluster assembly is gradual, allowing establishment of approximate pressure equilibrium (*Tan et al., 2006*).

On the smaller scales of protostellar cores, for bright embedded continuum sources, infall is inferred from red-shifted line profiles seen in absorption against the continuum (the blue-shifted inverse P-Cygni emission profile is difficult to distinguish from the continuum). In a few cases, this red-shifted absorption is observed in NH_3 at cm wavelengths against free-free emission of an embedded HC H II region (G10.62–0.38, *Sollins et al., 2005*, note *Keto, 2002* has also reported ionized gas infall in this source (§4.4); G24.78+0.08 A1, *Beltrán et al., 2006*). In other cases, it is observed with mm interferometers in CN , C^{34}S , ^{13}CO against core dust continuum emission (W51 N, *Zapata et al., 2008*; G19.61–0.23, *Wu et al., 2009*; G31.41+0.31, *Girart et al., 2009*; NGC 7538 IRS1, *Beuther et al., 2013b*). *Wyrowski et al.* (2012) saw absorption of rotational NH_3 transitions against FIR dust emission with *SOFIA*. For the interferometric observations, infall on scales of $\sim 10^3$ AU is traced. Infall speeds are a few km s^{-1} ; $\dot{M}_{\text{infall}} \sim 10^{-3} - 10^{-2} M_{\odot} \text{ yr}^{-1}$. *Goddi et al.* (2011a) used CH_3OH masers in AFGL 5142 to infer $\dot{M}_{\text{infall}} \sim 10^{-3} M_{\odot} \text{ yr}^{-1}$ on 300 AU scales. The above results indicate collapse of cores, in contrast to clumps, occurs rapidly, i.e., close to free-fall rates.

Dust continuum polarization is observed towards some massive protostars to infer B -field orientations (e.g., *Tang et al., 2009*; *Beuther et al., 2010b*; *Sridharan et al., 2014*). *Girart et al.*, (2009) observed a relatively ordered “hour-glass” morphology in G31.41+0.31, suggesting contraction has pinched the B -field. However, since the region studied is only moderately supercritical ($\Sigma \sim 5 \text{ g cm}^{-2}$ and plane of sky $B \sim 2.5 \text{ mG}$; *Frau, Girart & Beltrán, priv. comm.*), the field may still be dynamically important, e.g., in transferring angular momentum and suppressing fragmentation.

4.2. Accretion Disks

In Core Accretion models, the infall envelope is expected to transition from near radial infall to gradually greater degrees of rotational support, until near circular orbits are achieved in a disk. If the disk is massive, then one does not expect a Keplerian velocity field. Also, massive

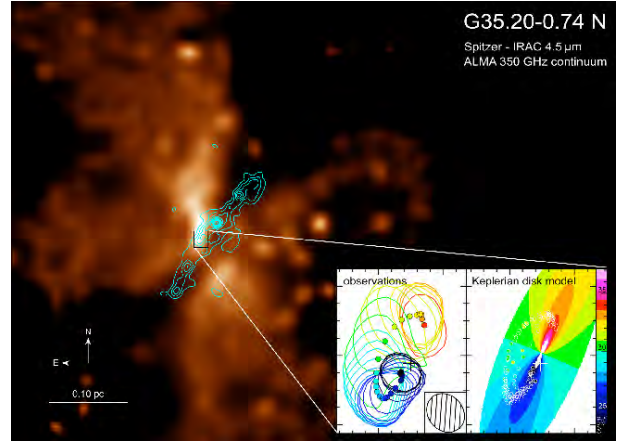


Fig. 6.— G35.20–0.74N massive protostar (*Sánchez-Monge et al., 2013a*). Large-scale image of $4.5 \mu\text{m}$ emission, expected to trace outflow cavities, with contours showing $850 \mu\text{m}$ continuum observed with *ALMA*. Left inset shows CH_3CN (19-18) $K=2$ emission peaks (solid circles; outer circle is 50% contour) from a 2D Gaussian fit channel by channel (velocity scale on right). Right inset compares these emission peaks with a Keplerian model.

moderately gravitationally unstable disks may form large-scale, perhaps lop-sided, spiral arms that may give the disk an asymmetric appearance (*Krumholz et al., 2007c*). Disk gravitational instability is a likely mechanism to form binaries or small- N multiples. Once the infall envelope has dispersed, either by feedback or exhaustion via accretion, then a remnant, lower-mass, near-Keplerian disk may persist for a time, until it also dissipates via feedback or accretion.

One of the simplest methods by which detection of accretion disks has been claimed is via imaging of a flattened NIR-extinction structure surrounding a NIR source (e.g., *Chini et al., 2004*; *Preibisch et al., 2011*). The latter authors report a 5500 AU diameter disk of $2 M_{\odot}$ around a $10 - 15 M_{\odot}$ star. However, in the absence of kinematic confirmation from molecular line observations, one must also consider the possibility of chance alignment of the source with a non-rotationally-supported filamentary dust lane.

Hot and warm dust in close, $\lesssim 100$ AU, proximity to the protostar, likely in a disk or outflow cavity wall, can sometimes be inferred from NIR or MIR interferometry (e.g., *Kraus et al., 2010*; *de Wit et al., 2011*; *Boley et al., 2013*). Most of the 24 MIR sources studied by *Boley et al.* show deviations from spherical symmetry, but it is difficult to tell if these are due primarily to disks or outflows.

For methods tracing kinematics, there are ~ 10 examples of “rotating toroids” in which velocity gradients traced by, e.g., C^{34}S , HDO , H^{18}O , or CH_3CN , have been seen on $\gtrsim \text{few} \times 1000$ AU scales that are perpendicular to protostellar outflows (§4.3) emerging from “hot cores” (§4.5) (*Cesaroni et al., 2007*; *Beltrán et al., 2011*). Most are probably in the process of forming B stars, such as AFGL 2591–VLA3 (*Wang et al., 2012*), but the sample also includes the UC H II regions G10.62–0.38 and G29.96–0.02 (*Beltrán et al., 2011*) with $m_* \gtrsim 15 M_{\odot}$. The disk reported by

Wang *et al.*, (2012) appears to have sub-Keplerian kinematics, together with an expanding component perhaps driven by the outflow. Keplerian rotation has been claimed for IRAS 20126+4104 (Cesaroni *et al.*, 2005) and G35.20–0.74N (Sánchez-Monge *et al.*, 2013a; Fig. 6). However, in the latter, where a $r_d \gtrsim 2500$ AU disk is inferred from an arc of centroid positions of sequential velocity channels of CH₃CN observed with ~ 1000 AU resolution, there is misalignment of the projected rotation axis with the N-S MIR and ionized jet, thought to define the outflow axis (Zhang *et al.*, 2013b; see §4.3). On smaller scales, usually in nearby, lower mass and luminosity ($\sim 10^4 L_\odot$) systems, there is also evidence of flattened structures with kinematic gradients perpendicular to outflows (e.g., Cep A HW2, Patel *et al.*, 2005; IRAS 16547-4247, Franco-Hernández *et al.*, 2009; IRAS 18162-2048, Fernández-López *et al.*, 2011, Carrasco-González *et al.*, 2012).

NIR spectroscopic observations of CO(2-0) bandhead emission, sometimes emerging via scattered light through outflow cavities, can provide information about protostellar and disk photospheres, where temperatures are ~ 2000 – 5000 K, i.e., scales \lesssim few AU (e.g., Bik and Thi, 2004; Davies *et al.*, 2010; Ilee *et al.*, 2013). With spectral resolutions $\gtrsim 10^4$, disk kinematics can begin to be resolved. In Ilee *et al.*'s study, all 20 sources can be fit with a Keplerian model. For radio source *I* in the Orion Kleinmann-Low (KL) region (e.g., Menten and Reid, 1995; Plambeck *et al.*, 2013), photospheric temperatures ~ 4500 K are inferred (Morino *et al.*, 1998; Testi *et al.*, 2010). Hosokawa and Omukai (2009) modeled this as emission from a very large $\sim 100 R_\odot$ protostar (swollen by high accretion rates), while Testi *et al.* (2010) preferred accretion disk models.

There are claims of massive protostellar accretion disks based on methanol masers (e.g., Pestalozzi *et al.*, 2009). However, characterization of disks by this method is hampered by the uncertain excitation conditions and nonlinear nature of the maser emission, together with possible confusion with outflow motions. In Cep A HW2 methanol masers appear to trace the outflow (Torstensson *et al.*, 2011). Note, Zeeman splitting of these maser lines allow *B*-field strengths (~ 20 mG) and morphologies (perpendicular to the disk) to be measured (Vlemmings *et al.*, 2010).

Spatially and kinematically well-resolved observations via thermal line emission from massive protostar disks remain lacking. This is not surprising if disk diameters are typically $\lesssim 1000$ AU (§2.3), i.e., $\lesssim 0.5''$ at 2 kpc. The high angular resolution to be achieved by ALMA in the coming years should provide breakthrough capabilities in this area.

4.3. Protostellar Outflows

Collimated, bipolar protostellar outflows (see also Frank *et al.*, this volume) have been observed from massive protostars, mostly via CO and HCO⁺, and their isotopologues, (e.g., Beuther *et al.*, 2002; Wu *et al.*, 2005a; Garay *et al.*, 2007; López-Sepulcre *et al.*, 2009). Correlations are seen between outflow power, force and mass loss rate, with bolo-

metric luminosity over a range $L \sim 0.1$ – $10^6 L_\odot$. This suggests outflows from massive protostars are driven in the same way as those from low-mass protostars, namely via magneto-centrifugal X- or disk-winds (momentum from radiation pressure, $\sim L/c$, is far too small; Wu *et al.*, 2005a).

Based on a tentative trend inferred from several sources, Beuther and Shepherd (2005; see also Vaidya *et al.*, 2011) proposed a scenario in which outflow collimation decreases with increasing protostellar mass, perhaps due to the increasing influence of quasi-spherical feedback (winds, ionization or radiation pressure). However, such evolution is also expected in models of disk-wind breakout from a self-gravitating core (Zhang *et al.*, 2014; see Fig. 3).

Study of SiO may help disentangle “primary” outflow (i.e., material launched from the disk) from “secondary” outflow (i.e., swept-up core/clump material). SiO may trace the primary outflow more directly, since its abundance is likely enhanced for the part of the disk-wind (and all the X-wind) launched from inside the dust destruction radius. However, SiO may also be produced in internal shocks in the outflow or at external shocks at the cavity walls. The single-dish survey of López-Sepulcre *et al.* (2011) found a decrease of the SiO luminosity with increasing luminosity-to-mass ratio in massive protostars (however, see Sánchez-Monge *et al.* 2013b). Interferometric SiO observations, necessary to resolve the structure of massive protostellar outflows, are relatively few and mostly focused on sources with $L < 10^5 L_\odot$ (e.g., AFGL 5142, Hunter *et al.*, 1999; IRAS 18264–1152, Qiu *et al.*, 2007; IRAS 18566+0408, Zhang *et al.*, 2007; G24.78+0.08, Codella *et al.*, 2013; IRAS 17233–3606, Leurini *et al.*, 2013). These have traced well-collimated jets, with collimation factors similar to those from low-mass protostars. For higher-mass protostars with $L > 10^5 L_\odot$, interferometric SiO observations are scarcer and collimation results inconclusive. Sollins *et al.*, (2004) mapped the shell-like UC H II region G5.89–0.39 with the SMA, finding a collimated SiO outflow, but the resolution was insufficient to distinguish the multiple outflows later detected in CO by Su *et al.* (2012). On the other hand, for IRAS 23151+5912 (Qiu *et al.*, 2007) and IRAS 18360–0537 (Qiu *et al.*, 2012), the molecular outflows traced by SiO are not well collimated and are consistent with ambient gas being entrained by an underlying wide-angle wind. Vibrationally excited SiO maser emission is thought to trace a wide-angle bipolar disk wind on scales of 10–100 AU around the massive protostar source *I* in Orion KL (e.g., Greenhill *et al.*, 2013).

Thermal (bremsstrahlung) radio jets should become prominent when the protostar contracts towards the main sequence (i.e., for $m_* \gtrsim 15 M_\odot$) causing its H-ionizing luminosity to increase dramatically. Shock ionization, including at earlier stages, is also possible (Hofner *et al.*, 2007). The primary outflow will be the first gas ionized, so cm continuum and radio recombination lines (RRLs) can trace massive protostar outflows. Elongated, sometimes clumpy, thermal radio continuum sources are observed around massive protostars: e.g., G35.20–0.74N (Gibb *et al.*, 2003);

IRAS 16562-3959 (*Guzmán et al.*, 2010). Many unresolved HC H II regions (§4.4) may be the central parts of ionized outflows, since the emission measure is predicted to decline rapidly with projected radius (*Tan and McKee*, 2003). Synchrotron radio jets are seen from some massive protostars, e.g., W3(H₂O) (*Reid et al.*, 1995) and HH 80–81 (*Carrasco-González et al.*, 2010), but why some have synchrotron emission while most others are thermal is unclear.

Outflows also manifest themselves via cavities cleared in the core. Cavity walls, as well as exposed disk surface layers, experience strong radiative, and possibly shock, heating, which drive astrochemical processes that liberate and create particular molecular species that can serve as further diagnostics of outflows, such as water and light hydrides (see §4.5) and maser activity (e.g., H₂O, CH₃OH) (e.g., *Ellingsen et al.*, 2007; *Moscadelli et al.*, 2013). High-J CO lines are another important tracer of this warm, dense gas (*Fuente et al.*, 2012; *Yıldız et al.*, 2013; *San José-García et al.*, 2013). Densities and temperatures of outflowing gas in AFGL 2591 have been measured by CO and other highly excited linear rotors (*van der Wiel et al.*, 2013).

Given the high extinctions, outflow cavities can be the main escape channel for MIR (and even some FIR) radiation, thus affecting source morphologies. *De Buizer* (2006) proposed this explains the 10 & 20 μm appearance of G35.20–0.74N, where only the northern outflow cavity that is inclined towards us (and is aligned with the northern radio jet) is prominent in ground-based imaging. *Zhang et al.* (2013b) observed this source with *SOFIA* at wavelengths up to $\sim 40 \mu\text{m}$ and detected the fainter counter jet. Comparing with Core Accretion RT models, they estimated the protostar has $m_* \sim 20 - 34 M_\odot$, embedded in a core with $M_c = 240 M_\odot$, in a clump with $\Sigma_{\text{cl}} \simeq 0.4 - 1 \text{ g cm}^{-2}$.

While much MIR emission from outflow cavities is due to thermal heating of cavity walls, in the NIR a larger fraction is emitted from the protostar and inner disk/outflow, reaching us directly or via scattering. The Br γ line and rovibrational H₂ lines in the NIR can reveal information about the inner outflow (e.g., *Cesaroni et al.*, 2013). Polarization vectors from scattered light can help localize the protostar: e.g., in Orion KL at 4 μm (*Werner et al.*, 1983) these vectors point to a location consistent with radio source *I*.

The Orion KL region also serves as an example of the rare class of “explosive” outflows. Forming the inner part of the outflow from KL, is a wide-angle flow containing “bullets” of NIR H₂ and Fe line emission (*Allen and Burton*, 1993; *Bally et al.*, 2011). Their spectra and kinematics yield a common age of $\sim 10^3$ yr. A 10^4 yr-old example of such a flow has been claimed by *Zapata et al.* (2013) in DR21. The KL outflow has been interpreted as being due to tidally-enhanced accretion and thus outflow activity from the close ($\sim \text{few} \times 10^2$ AU) passage near source *I* of the Becklin-Neugebauer (BN) runaway star, itself ejected from interaction with the $\theta^1 C$ binary in the Trapezium (*Tan*, 2004). BN’s ejection from $\theta^1 C$ has left a distinctive dynamical fingerprint on $\theta^1 C$, including recoil motion, orbital binding energy and eccentricity—properties unlikely (prob-

ability $\lesssim 10^{-5}$) to arise by chance (*Chatterjee and Tan*, 2012). This scenario attributes the “explosive” outflow as being the perturbed high activity state of a previously normal massive protostellar outflow (akin to an FU Orionis outburst, but triggered by an external encounter rather than an internal disk instability). Alternatively, *Bally and Zinnecker* (2005) and *Goddi et al.* (2011b) proposed BN was ejected by source *I*, which must then be a hard binary or have suffered a merger. This would imply much closer, disruptive dynamical interactions involving the massive protostar(s) at source *I* (*Bally et al.*, 2011). In either scenario, recent perturbation of gas on $\sim 10^2 - 10^3$ AU scales around source *I* has occurred, likely affecting observed hot core complexity (*Beuther et al.*, 2006) and interpretation of maser disk and outflow kinematics (*Greenhill et al.*, 2013).

4.4. Ionized Gas

Observationally, HC and UC H II regions are defined to have sizes < 0.01 pc and < 0.1 pc, respectively (*Beuther et al.*, 2007; *Hoare et al.*, 2007). They have rising radio spectral indices, due to thermal bremsstrahlung emission from $\sim 10^4$ K plasma. A large fraction of HC H II regions show broad (FWHM $\gtrsim 40 \text{ km s}^{-1}$) RRLs (*Sewilo et al.*, 2011). Studies of Brackett series lines in massive protostars also show broad lines, perhaps consistent with disk or wind kinematics (*Lumsden et al.*, 2012). Demographics of the UC H II region population imply a lifetime of $\sim 10^5$ yr (*Wood and Churchwell*, 1989; *Mottram et al.*, 2011), much longer than the expansion time at the ionized gas sound speed, so a confinement or replenishment mechanism is needed.

The above observational classification may mix different physical states that are expected theoretically during massive star formation (§2.3 & 2.4). An outflow-confined H II region (*Tan and McKee*, 2003) is expected first, appearing as a radio jet that gradually opens up as the entire primary-outflow-filled cavity is ionized. Together with outflow feedback, ionization should then start to erode the core infall envelope, driving a photoevaporative flow. Strongly-bound parts of the core may become ionized yet continue to accrete (*Keto*, 2007), as inferred in G10.62–0.38 by *Keto* (2002) and W51e2 by *Keto and Klaassen* (2008). Eventually, remnant equatorial accretion may continue to feed a disk that is subject to photoevaporation (§2.4).

Since massive star ionizing luminosities vary by factors ~ 100 from B to O stars (Fig. 2), H II region sizes will also vary. So while, in general, one expects earlier phases of accretion to be associated with smaller H II regions, it is possible some UC H II regions still harbor accreting massive protostars, while some HC H II regions host non-accreting, already-formed B stars in dense clump environments.

Using the Red MSX Source (RMS) survey (*Lumsden et al.*, 2013) and comparing with main sequence lifetimes, *Mottram et al.* (2011) derived lifetimes of radio-quiet (RQ) massive protostars (likely the accretion phase before contraction to the ZAMS; Fig. 2) and “compact” (including UC) H II regions as a function of source luminosity. RQ massive protostars have lifetimes $\simeq 5 \times 10^5$ yr for $L \simeq$

$10^4 L_{\odot}$, declining to $\simeq 1 \times 10^5$ yr for $L \simeq 10^5 L_{\odot}$. No RQ massive protostars were seen with $L \gg 10^5 L_{\odot}$, consistent with Fig. 2: by this luminosity most protostars should have contracted to the ZAMS and thus become “radio-loud” (for $\Sigma_{\text{cl}} \lesssim 3 \text{ g cm}^{-2}$). The “compact” H II regions have lifetimes $\simeq 3 \times 10^5$ yr (independent of L). *Davies et al.* (2011) extended this work to show that the data favor models in which the accretion rate to massive protostars increases with time, as expected in the fiducial Turbulent Core Accretion model (MT03) with $k_{\rho} = 1.5$ and with accretion rates appropriate for $\Sigma_{\text{cl}} \sim 1$. However, their derived trend of increasing accretion rates is also compatible with the Competitive Accretion model of *Bonnell et al.* (2001).

4.5. Astrochemistry of Massive Protostars

Massive protostars significantly affect the chemical composition of their surroundings. Firstly, they heat gas and dust, leading to sublimation of icy mantles formed during the cold PSC phase (e.g., *Charnley et al.*, 1992; *Caselli et al.*, 1993)—the hot core phase. Secondly, they drive outflows that shock the gas enabling some reactions with activation energies and endothermicities to proceed (e.g., *Neufeld and Dalgarno*, 1989). Knowledge of chemical processes is vital to understand the regions traced by the various molecular lines and thus to study the structure and dynamics of the gas surrounding the protostar, i.e., its infall envelope, disk and outflow (e.g., *Favre et al.*, 2011; *Bisshop et al.*, 2013), fundamental to test formation theories. Unfortunately, the chemistry in these regions is based heavily on poorly known surface processes, so it is important to keep gathering high sensitivity and spectral/angular resolution data to constrain astrochemical theory, as well as laboratory data to lessen the uncertainties in the rate and collisional coefficients required in astrochemical and RT codes.

The majority of chemical models of these early stages of massive protostellar evolution do not take into account shocks and focus on three main temporal phases (see review by *Herbst and van Dishoeck*, 2009): (i) cold phase ($T \sim 10$ K), before protostar formation, where freeze-out, surface hydrogenation/deuteration and gas-phase ion-neutral reactions are key processes. The main constituents of icy mantles are H_2O , followed by CO & CO_2 , and then by CH_3OH , NH_3 & CH_4 (*Öberg et al.*, 2011), as O, C, N & CO are mainly hydrogenated, since H is by far the fastest element on the surface at such low temperatures; (ii) warm-up phase, when the protostar starts to heat the surroundings and temperatures gradually increase from ~ 10 to $\gtrsim 100$ K (e.g., *Viti et al.*, 2004); (iii) hot core phase, when all mantles are sublimated and only gas phase chemistry proceeds (e.g., *Brown et al.*, 1988). The warm-up phase is thought to be critical for surface formation of complex molecules (*Garrod and Herbst*, 2006). *Öberg et al.* (2013) claim their observations of N- and O-bearing organics toward high-mass star-forming region NGC 7538 IRS9 are consistent with the onset of complex chemistry at 25-30 K. At these dust temperatures, hydrogen atoms evaporate, while heavier species

and molecules can diffuse more quickly within the mantles and form species more complex than in the cold phase. *Garrod* (2013) showed glycine can form in ice mantles at temperatures between 40 and 120 K and be detected in hot cores with *ALMA*. *Aikawa et al.* (2012) coupled a comprehensive gas-grain chemical network with 1D hydrodynamics, also showing that complex molecules are efficiently formed in the warm-up phase. Early complex molecule formation in the cold phase, perhaps driven by cosmic ray induced UV photons or dust heating (*Bacmann et al.*, 2012), may need to be included in the above models.

Herschel has discovered unexpected chemistry in massive star-forming regions. Light hydrides such as OH^+ and H_2O^+ , never observed before, have been detected in absorption and weak emission toward W3 IRS5, tracing outflow cavity walls heated and irradiated by protostellar UV radiation (e.g., *Benz et al.*, 2010; *Bruderer et al.*, 2010).

Water abundance and kinematics have been measured towards several massive star-forming regions, with different hot cores showing a variety of abundance levels. *Neill et al.* (2013) found abundances of $\sim 6 \times 10^{-4}$ toward Orion KL (making H_2O the predominant repository of O) and a relatively large $\text{HDO}/\text{H}_2\text{O}$ ratio (~ 0.003), while *Emprechtinger et al.*, (2013) measured 10^{-6} H_2O abundance and $\text{HDO}/\text{H}_2\text{O} \sim 2 \times 10^{-4}$ in NGC 6334 I. Thus, evaporation of icy mantles may not always be complete in hot cores, unlike the assumption made in astrochemical models. It also suggests that the level of deuteration is different in the bulk of the mantle compared to the upper layers that are first returned to the gas phase (*Kalvāns and Shmed*, 2013; *Taquet et al.*, 2013), or that these two hot cores started from slightly different initial dust temperatures, which may highly affect water deuteration (*Cazaux et al.*, 2011). Water vapour abundance has also been found to be low in the direction of outflows (7×10^{-7} ; *van der Tak et al.*, 2010), again suggesting ice mantles are more resistant to destruction in shocks than previously thought. The low water abundances in the outer envelopes of massive protostars (e.g., 2×10^{-10} in DR21, *van der Tak et al.*, 2010; 8×10^{-8} in W43-MM1, *Herpin et al.*, 2012) are likely due to water being mostly in solid form.

4.6. Comparison to Lower-Mass Protostars

Some continuities and similarities were already noted between high and low-mass starless cores, including the continuous, power-law form of the CMF (though work remains to measure the pre-stellar CMF) and the chemical evolution of CO freeze-out and high deuteration of certain species. Differences include massive starless cores having larger nonthermal internal motions, though these are also being found in lower-mass cores in high-mass star-forming regions (*Sánchez-Monge et al.*, 2013c). Massive cores may also tend to have higher Σ_s (§4.7), whereas low-mass cores can be found with a wider range down to lower values.

For low-mass protostars, an evolutionary sequence from PSCs to pre-main sequence stars was defined by *Lada* (1991) and *André* (1995): Class 0, I, II, and III objects based

on SEDs. As described above, an equivalent sequence for massive protostars is not well established. Core and Competitive Accretion models predict different amounts and geometries of dense gas and dust in the vicinity of the protostar. Even for Core Accretion models (and also for low-mass protostars), the SED will vary with viewing angle for the same evolutionary stage. For a given mass accretion rate and model for the evolution of the protostar and its surrounding disk and envelope, the observed properties of the system can be calculated. Examples of such models include those of *Robitaille et al.* (2006), *Molinari et al.* (2008), and *Zhang et al.*, (2014; see Figs. 2 and 3).

For massive protostars one expects a “radio-quiet” phase before contraction to the ZAMS. A growing region, at first confined to the disk and outflow, is heated to $\gtrsim 100$ K, exhibiting hot core chemistry. Protostellar outflows are likely to have broken out of the core, and be gradually widening the outflow cavities. Up to this point, the evolution of lower mass protostars is expected to be qualitatively similar. Contraction to the ZAMS leads to greatly increased H-ionizing luminosities and thus a “radio-loud” phase, corresponding to HC or UC H II regions. Hot core chemistry will be more widespread, but there will also now be regions (perhaps confined to the outflow and disk surfaces) that are exposed to high FUV radiation fields. Stellar winds from the ZAMS protostar should become much stronger than those from low-mass protostars, especially on crossing the “bistability jump” at $T_* \simeq 21,000$ K (*Vink et al.*, 2001).

How do observed properties of lower-mass protostars compare with massive ones? Helping address this are studies of “intermediate-mass” protostars with $L \sim 100 - 10^4 L_\odot$ and sharing some characteristics of their more massive cousins (e.g., clustering, creation of photo-dissociation regions). Many are closer than 1 kpc, allowing determination of the physical and chemical structures at similar spatial scales as in well-studied low-mass protostars.

For disks, while there are examples inferred to be present around massive protostars (§4.2), information is lacking about their resolved structure or even total extent, making comparison with lower-mass examples difficult. Most massive protostellar disks appear to have sizes $\lesssim 10^3$ AU. If disk size is related to initial core size, then one expects $r_d \propto R_c \propto (M_c/\Sigma_{cl})^{1/2}$, so larger disks resulting from more massive cores may be partly counteracted if massive cores tend to be in higher Σ_{cl} clumps. If stronger magnetization is needed to support more massive cores, then this may lead to more efficient magnetic braking during disk formation. Survival of remnant disks around massive stars may be inhibited by more efficient feedback (§2.4).

Comparison of outflow properties was discussed in §4.3, noting the continuity of outflow force and mass loss rates with L . Similar collimation factors are also seen, at least up to $L \sim 10^5 L_\odot$. The rare “explosive” outflows may affect massive protostars more than low-mass ones, but too few examples are known to draw definitive conclusions.

Equivalent regions exhibiting aspects of hot core chemistry, e.g., formation of complex organic molecules, have

been found around low-mass (e.g., IRAS 16293–2422: *Cazaux et al.* 2003) and intermediate-mass (e.g., IC 1396N, *Fuente et al.*, 2009; NGC 7129, *Fuente et al.*, 2012; IRAS 22198+6336 & AFGL 5142 [also discussed in §4.1 & 4.3], *Palau et al.*, 2011) protostars. Around low-mass protostars these regions appear richer in O-bearing molecules like methyl-formate (CH_3OOCH) and poorer in the N-bearing compounds. They have high deuteration fractions (e.g., *Demyk et al.*, 2010) unlike hot cores around massive protostars. The situation in intermediate-mass protostars is mixed: IRAS 22198+6336 and AFGL 5142 are richer in oxygenated molecules while NGC 7129 is richer in N-species. The recent detection of the vibrationally excited lines of CH_3CN and HC_3N in this hot core also points to a higher gas temperature (*Fuente et al.*, in prep.). *Palau et al.* (2011) discussed that these hot cores can encompass two different types of regions, inner accretion disks and outflow shocks, helping to explain the observed diversity.

Finally, the stellar IMF for $m_* \gtrsim 1 M_\odot$ appears well-described by a continuous and universal power law (see §5), with no evidence of a break that might evidence a change in the physical processes involved in star formation.

In summary, many aspects of the star formation process appear to either be very similar or vary only gradually as a function of protostellar mass. While some of these properties remain to be explored at the highest masses, we conclude that the bulk of existing observations support a common star formation mechanism from low to high masses.

4.7. Conditions for Massive Star Formation

Do clumps that form massive stars require a threshold Σ or other special properties? *López-Sepulcre et al.* (2010) found an increase in outflow detection rate from 56% to 100% when bisecting their clump sample by a threshold of $\Sigma_{cl} = 0.3 \text{ g cm}^{-2}$. This is a factor of a few smaller than the threshold predicted by *Krumholz and McKee* (2008) from protostellar heating suppression of fragmentation of massive cores (§2.4), and thus consistent within the uncertainties in deriving Σ . However, this clump sample contains a mixture of IR-dark and bright objects spanning this threshold, whereas one expects protostellar heating to be associated with IR-bright objects. *Longmore et al.* (2011) estimated the low-mass stellar population needed to be responsible for the observed temperature structure in the fragmenting clump G8.68–0.37, concluding it is too large compared to that allowed by the clump’s bolometric luminosity. *BT12* found relatively low values of $\Sigma_{cl} \sim 0.3 \text{ g cm}^{-2}$ in their IRDC sample and advocated magnetic suppression of fragmentation. *Kauffmann et al.* (2010) found three clouds that contain massive star formation (Orion A, G10.15–0.34, G11.11–0.12) satisfy $M(r) \geq 870 r_{pc}^{4/3} M_\odot$, while several clouds not forming massive stars do not. This empirical condition is equivalent to $\Sigma \geq 0.054 M_3^{-1/2} \text{ g cm}^{-2}$, i.e., a relatively low threshold that may apply to the global clump even though massive stars form in higher Σ peaks. In summary, more work is needed to better establish if there are

minimum threshold conditions for massive star formation. This is difficult since once one is sure a massive star is forming, it will have altered its environment. Thus it may be more fruitful studying the formation requirements of massive PSCs, though there are currently very few examples (§3).

5. RELATION TO STAR CLUSTER FORMATION

5.1. The Clustering of Massive Star Formation

de Wit et al. (2005) studied Galactic field O stars, concluding that the fraction born in isolation was low ($4 \pm 2\%$). *Bressert et al.* (2012) have found a small number of O stars that appear to have formed in isolation in the 30 Dor region of the LMC, while *Selier et al.* (2011) and *Oey et al.* (2013) have presented examples in the SMC. For the Galactic sample, the low fraction of “isolated-formation” O stars could be modeled by extrapolating a stochastically-sampled power-law initial cluster mass function (ICMF) down to very low masses, including “clusters” of single stars. Such a model suggests that massive star formation is not more clustered than lower-mass star formation and that the “clustering” of star formation does not involve a minimum threshold of cluster mass or density (see also *Bressert et al.* 2010).

The question of whether massive stars tend to form in the central regions of clumps/clusters is difficult to answer. Observationally, there is much evidence for the central concentration of massive stars within clusters (e.g., *Hillenbrand*, 1995; *Qiu et al.*, 2008; *Kirk and Myers*, 2012; *Pang et al.*, 2013; *Lim et al.*, 2013). For clusters, like the ONC, where a substantial fraction of the initial gas clump mass has formed stars, dynamical evolution leading to mass segregation during star cluster formation may overwhelm any signature of primordial mass segregation (e.g., *Bonnell and Davies*, 1998; *Allison and Goodwin*, 2011; *Maschberger and Clarke*, 2011), especially if cluster formation extends over many local dynamical times (*Tan et al.*, 2006). This problem is even more severe in gas-free, dynamically-older systems like NGC 3603, Westerlund 1 and the Arches.

Earlier phase studies are needed. *Kumar et al.* (2006) searched 2MASS images for clusters around 217 massive protostar candidates, finding 54. Excluding targets most affected by Galactic plane confusion, the detection rate was $\sim 60\%$. *Palau et al.* (2013) studied 57 (mm-detected) cores in 18 “protoclusters”, finding quite low levels of fragmentation and relatively few associated NIR/MIR sources.

Do massive stars tend to form earlier, later or contemporaneously with lower-mass stars? In Turbulent Core Accretion (MT03), the formation times of stars from their cores show a weak dependence with mass, $t_{*f} \propto m_{*f}^{1/4}$, and the overall normalization is short compared to the global cluster formation time, if that is spread out over at least a few free-fall times. Competitive Accretion models (e.g., *Wang et al.*, 2010) involve massive stars gaining their mass gradually over the same timescales controlling global clump evolution, suggesting that massive stars would form later than typical low-mass stars. Systematic uncertainties in young stellar age estimates (*Soderblom et al.*, this volume) make

this a challenging question to answer. In the ONC, *Da Rio et al.* (2012) have shown there is a real age spread of a few Myr, i.e., at least several mean free-fall times, but no evidence for a mass-age correlation. Massive stars are forming today in the ONC, i.e., source I. If the runaway stars μ Col and AE Aur, together with the resulting binary, ι Ori, were originally in the ONC about 2.5 Myr ago (*Hoogerwerf et al.*, 2001), then massive stars appear to have formed contemporaneously with the bulk of the cluster population.

5.2. The IMF and Binarity of Massive Stars

The massive star IMF and its possible variation with environment are potential tests of formation mechanisms. The IMF is constrained by observations of massive stars in young clusters, especially “super star clusters” (SSCs) with $M_* \gtrsim 10^4 M_\odot$ where effects of incomplete statistical sampling are reduced. E.g., for IMF $dN/dm_* \propto m_*^{-\alpha_*}$ and $\alpha_* = 2.35$ (Salpeter) from $m_{*l} = 0.1 M_\odot$ to upper truncation mass of $m_{*u} = 100$ or $1000 M_\odot$, the median expected maximum stellar mass in a cluster with $M_* = 10^4 M_\odot$ is 83.6, 226 M_\odot , respectively (e.g., *McKee and Williams*, 1997). For $M_* = 10^5 M_\odot$ it is 98.0, 692 M_\odot , respectively.

Estimates of m_{*u} range from $\simeq 150 M_\odot$ (e.g., *Figer*, 2005) to $\simeq 300 M_\odot$ (*Crowther et al.*, 2010), with uncertainties due to crowding, unresolved binarity, extinction corrections and the NIR magnitude-mass relation. Also, a limiting m_{*u} arising from star formation may occasionally appear to be breached by mergers or mass transfer in binary systems (e.g., *Banerjee et al.*, 2012; *Schneider et al.*, 2014). It is not yet clear if m_{*u} is set by local processes (e.g., ionization or radiation pressure feedback (§2.4, §2.5), rapid mass loss due to stellar instability) or by the cluster environment (e.g., *Weidner et al.*, 2013; however, see *Krumholz*, 2014).

Deriving initial stellar masses can thus require modeling stellar evolution, including the effects of rotation, mass loss and binary mass transfer (e.g., *Sana et al.*, 2012; *De Mink et al.*, 2013; *Schneider et al.*, 2014). Dynamical evolution in clusters leads to mass segregation and ejection of stars, further complicating IMF estimation from observed mass functions (MFs) of either current or initial stellar masses.

Many attempts have been made to derive MFs in SSCs. For Westerlund 1, the most massive young cluster in the Galaxy, *Lim et al.* (2013) find $\alpha_* = 1.8 \pm 0.1$ within $r < 2.8$ pc over mass range $5 < m_*/M_\odot < 85$, and an even shallower slope of $\alpha_* = 1.5$ if the statistically incomplete highest-mass bins are excluded. A similar slope of $\alpha_* = 1.9 \pm 0.15$ for $1 < m_*/M_\odot < 100$ is measured for proper-motion members in the central young cluster of NGC 3603, with an even shallower slope of $\alpha_* = 1.3 \pm 0.3$ found in the cluster core for the intermediate- to high-mass stars ($4 < m_*/M_\odot < 100$, *Pang et al.*, 2013). For R136 in 30 Doradus in the LMC, *Andersen et al.* (2009) find $\alpha_* = 2.2 \pm 0.2$ for $1 < m_{*f}/M_\odot < 20$ and a radial coverage of 3 to 7 pc. However, the cluster core remains poorly resolved and its MF uncertain. In NGC 346 in the SMC, *Sabbi et al.* (2008) find $\alpha_* = 2.43 \pm 0.18$ for $0.8 < m_{*f}/M_\odot < 60$.

Environmental conditions of temperature, cosmic ray

flux, magnetization and orbital shear are all higher in the Galactic center, so one may expect IMF variations (e.g., *Morris and Serabyn*, 1996). In the Quintuplet cluster core, $r < 0.5\text{pc}$, the present-day MF is found to be $\alpha_* = 1.7 \pm 0.2$ for $4 < m_{*f}/M_\odot < 48$ (*Hußmann et al.*, 2012). As in Westerlund 1 and NGC 3603, a steepening of the IMF slope with distance from cluster center is observed with $\alpha_* = 2.1 \pm 0.2$ for radii 1.2 to 1.8 pc, close to the expected tidal radius (*B. Hußmann*, priv. comm.). The core of the Arches cluster, also exhibits a relatively shallow MF, but the combined MF slope out to the tidal radius is $\alpha_* = 2.5 \pm 0.2$ for $15 < m_{*f}/M_\odot < 80$ (*Habibi et al.*, 2013).

Detailed N-body simulations have been carried out to model the Arches Cluster (e.g., *Harfst et al.*, 2010). The excellent match between the radial variation of the MF in these simulations and the observed increase in the MF slope with radius provide strong evidence that the steepening is caused by dynamical mass segregation alone. By analogy, the relatively shallow slopes observed in the central regions of all the above young, massive clusters are likely influenced, and possibly completely caused, by internal dynamical evolution of these clusters on timescales as short as 1-3 Myr, within the current ages of these clusters.

The most extreme star-forming environment resolved to date is the young nuclear cluster surrounding the supermassive black hole SgrA* in the center of the Milky Way. If the effects of increased tidal shear and temperatures cause an increase in the Jeans mass, it should most likely be observed in this environment. Previous studies suggested a slope as shallow as $\alpha_* = 0.45 \pm 0.3$ for $m_* > 10 M_\odot$ and with a truncation of $m_{*u} \simeq 30 M_\odot$, and hence proposed the most extreme stellar MF observed in a resolved population to date (*Bartko et al.*, 2010). Many of the young stars in the nuclear cluster are in an elongated disk-like structure (e.g., *Paumard et al.*, 2006), and optimizing for the inclusion of young disk candidates as members of the cluster revises this picture. Employing *Keck* spectroscopy along the known disk of young stars, *Lu et al.* (2013) found a slope of $\alpha_* = 1.7 \pm 0.2$ from detailed Bayesian modeling to derive individual stellar masses. While still flatter than the Salpeter slope, this result is now in agreement with the shape of the MFs found in the central regions of all other young, massive clusters outside of this very extreme environment. The effects of mass segregation and ejection for altering the observed MF are not very well known. Modulo these uncertainties, there is no evidence for IMF variation in the Galactic center compared to other massive clusters.

In summary, the massive young clusters resolved to date exhibit somewhat shallow present-day MFs in their cluster cores, with a steepening of the MF observed towards larger radii. Numerical simulations suggest that the central top-heavy mass distribution can be explained by mass segregation, and is not evidence for a deviating IMF in the high-mass regime. The fact that there is little or no variation of the shape of the high-mass IMF from NGC 346 to the Arches or Westerlund 1 suggests that the process of massive star formation has a very weak dependence on density,

which varies by two to three orders of magnitude between these clusters (Fig. 1). This implies stellar collisions are not important for forming massive stars in these environments, in agreement with theoretical estimates of collision rates by, e.g., *Moeckel and Clarke* (2011). Predictions of the dependence of the IMF with density are needed from simulations and models of Core and Competitive Accretion.

The binary properties of massive stars have been discussed extensively by *Zinnecker and Yorke* (2007) (see also *Sana et al.*, 2012; *De Mink et al.*, 2013). They are more likely to be in binary or multiples than lower-mass stars. For stars in cluster centers, these properties may also have been affected by dynamical evolution via interactions (e.g., *Parker et al.* 2011; *Allison and Goodwin*, 2011), which tend to harden and increase the eccentricity of binary orbits and can also lead to ejection of runaway stars. For example, such an interaction has been proposed to explain the properties of the θ^1 C binary near the center of the ONC (*Chatterjee and Tan*, 2012). Thus, one should be cautious using the observed binary properties of massive stars to constrain massive star formation theories, with attention to be focussed on objects that are either very young (i.e., still forming) or relatively isolated in lower-density environments.

6. CONCLUSIONS AND FUTURE OUTLOOK

It is a challenge to understand the wide variety of interlocking physical and chemical processes involved in massive star formation. Still, significant theoretical progress is being made in modeling these processes, both individually and in combination in numerical simulations. However, such simulations still face great challenges in being able to adequately resolve the scales and processes that may be important, including MHD-driven outflows, radiative feedback and astrochemistry. There are also uncertainties in how to initialize these simulations. Accurate prediction of the IMF, including massive stars, of a cluster forming under given environmental conditions remains a distant goal.

Close interaction with observational constraints is essential. Here rapid progress is also being made and, with the advent of *ALMA*, this should only accelerate. One challenge is development of the astrochemical sophistication needed to decipher the rich variety of diagnostic tracers becoming available for both pre- and protostellar phases. Determination of pre-stellar core mass functions and resolution of massive protostellar accretion disks, including possible binary formation, and outflows are important goals.

Core and Competitive Accretion theories are being tested by both simulation and observation. Core Accretion faces challenges of understanding fragmentation properties of magnetized, turbulent gas, following development of accretion disks and outflows from collapsing cores, and assessing the importance of external interactions in crowded cluster environments. Competitive Accretion is also challenged by theoretical implementation of realistic feedback from MHD outflows and by observations of massive starless cores, together with apparent continuities and similarities

of the star formation process across protostellar mass and luminosity distributions. There is much work to be done!

Acknowledgments. We thank S. Kong, A. Myers, Á. Sánchez-Monge, Y. Zhang for figures and discussions, and H. Beuther, M. Butler, P. Clark, N. Da Rio, M. Hoare, P. Klaassen, P. Kroupa, W. Lim & a referee for discussions.

REFERENCES

- Aikawa Y., Wakelam V. et al. (2012) *Astrophys. J.*, 760, 40.
 Allen D. A. and Burton M. G. (1993) *Nature*, 363, 54.
 Allison R. J. and Goodwin S. P. (2011) *Mon. Not. R. Astron. Soc.*, 415, 1967.
 Andersen M., Zinnecker H. et al. (2009) *Astrophys. J.*, 707, 1347.
 André P. (1995) *Astrophysics and Space Science*, 224, 29.
 Bacmann A., Taquet V. et al. (2012) *Astron. Astrophys.*, 541, L12.
 Bally J., Cunningham N. J. et al. (2011) *Astrophys. J.*, 727, 113.
 Bally J. and Zinnecker H. (2005) *Astron. J.*, 129, 2281.
 Banerjee S. et al. (2012) *Mon. Not. R. Astron. Soc.*, 426, 1416.
 Barnes P. J. et al. (2011) *Astrophys. J. Suppl.*, 196, 12.
 Barnes P. J. et al. (2010) *Mon. Not. R. Astron. Soc.*, 402, 73.
 Bartko H., Martins F. et al. (2010) *Astrophys. J.*, 708, 834.
 Battersby C., Bally J. et al. (2011) *Astron. Astrophys.*, 535, 128.
 Bate M. R. (2012) *Mon. Not. R. Astron. Soc.*, 419, 3115.
 Bate M. R. et al. (1995) *Mon. Not. R. Astron. Soc.*, 277, 362.
 Baumgardt H. and Klessen R. S. (2011) *Mon. Not. R. Astron. Soc.*, 413, 1810.
 Beltrán M. T., Cesaroni R. et al. (2006) *Nature*, 443, 427.
 Beltrán M. T. et al. (2011) *Astron. Astrophys.*, 525, 151.
 Benz A. O. et al. (2010) *Astron. Astrophys.*, 521, L35.
 Berger M. J. and Olinger J. (1984) *J. Comp. Phys.*, 53, 484.
 Bergin E. A. and Tafalla M. (2007) *Ann. Rev. Astron. Astrophys.*, 45, 339.
 Bertoldi F. and McKee C. F. (1992) *Astrophys. J.*, 395, 140.
 Beuther H., Schilke P. et al. (2002) *Astron. Astrophys.*, 383, 892.
 Beuther H. and Schilke P. (2004) *Science*, 303, 1167.
 Beuther H. and Shepherd D. S. (2005) *Cores to Clusters* (M. Kumar et al.), Springer, New York, p105-119.
 Beuther H., Zhang Q. et al. (2006) *Astrophys. J.*, 636, 323.
 Beuther H., Churchwell E. B., McKee C. F. and Tan J. C. (2007) *PPV* (B. Reipurth et al.), Univ. Arizona, Tucson, p165-180.
 Beuther H. et al. (2010a) *Astron. Astrophys.*, 518, L78.
 Beuther H. et al. (2010b) *Astrophys. J.*, 724, L113.
 Beuther H. et al. (2012) *Astron. Astrophys.*, 538, 11.
 Beuther H., Linz H. et al. (2013a) *Astron. Astrophys.*, 553, 115.
 Beuther H., Linz H. et al. (2013b) *Astron. Astrophys.*, 558, 81.
 Bik A. and Thi W. F. (2004) *Astron. Astrophys.*, 427, L13.
 Bisbas T. G. et al. (2009) *Astron. Astrophys.*, 497, 649.
 Bisschop S. E. et al. (2013) *Astron. Astrophys.*, 552, 122.
 Blandford R. D. and Payne D. G. (1982) *Mon. Not. R. Astron. Soc.*, 199, 883.
 Boley P. A., Linz H. et al. (2013) *Astron. Astrophys.*, 558, 24.
 Bonnell I. A. and Bate M. R. (2005) *Mon. Not. R. Astron. Soc.*, 362, 915.
 Bonnell I. A. et al. (2001), *Mon. Not. R. Astron. Soc.*, 323, 785.
 Bonnell I. A. et al. (1998) *Mon. Not. R. Astron. Soc.*, 298, 93.
 Bonnell I. A. and Davies M. B. (1998) *Mon. Not. R. Astron. Soc.*, 295, 691.
 Bonnell I. A. et al. (2004) *Mon. Not. R. Astron. Soc.*, 349, 735.
 Bonnell I. A., Larson R. B. & Zinnecker H. (2007) *PPV* (B. Reipurth et al.), Univ. Arizona, Tucson, p149-164.
 Bontemps S., Motte F. et al. (2010) *Astron. Astrophys.*, 524, 18.
 Bressert E. et al. (2012) *Astron. Astrophys.*, 542, 49.
 Bressert E. et al. (2010) *Mon. Not. R. Astron. Soc.*, 409, L54.
 Bromm V. (2013) *Rep. Prog. Phys.*, 76, 11.
 Brown P. D. et al. (1988) *Mon. Not. R. Astron. Soc.*, 231, 409.
 Bruderer S. et al. (2010) *Astron. Astrophys.*, 521, L44.
 Butler M. J. and Tan J. C. (2009) *Astrophys. J.*, 696, 484.
 Butler M. J. and Tan J. C. (2012) *Astrophys. J.*, 754, 5. [BT12]
 Carrasco-González C. et al. (2010) *Science*, 330, 1209.
 Carrasco-González C. et al. (2012), *Astrophys. J.*, 752, L29.
 Caselli P. and Myers P. C. (1995) *Astrophys. J.*, 446, 665.
 Caselli P., Hasegawa T. et al. (1993) *Astrophys. J.*, 408, 548.
 Caselli P., Vastel C. et al. (2008) *Astron. Astrophys.*, 492, 703.
 Caselli P., Walmsley C. M. et al. (1999) *Astrophys. J.*, 523, L165.
 Caselli P., Walmsley C. M. et al. (2002) *Astrophys. J.*, 565, 344.
 Cazaux S., Caselli P. et al. (2011) *Astrophys. J.*, 741, L34.
 Cazaux S., Tielens A. et al. (2003) *Astrophys. J.*, 593, L51.
 Cesaroni R., Galli D., Lodato G. et al. (2007) *Protostars and Planets V* (B. Reipurth et al., eds.), p197, Univ. of Arizona, Tucson.
 Cesaroni R., Massi F. et al. (2013) *Astron. Astrophys.*, 549, 146.
 Cesaroni R., Neri R. et al. (2005) *Astron. Astrophys.*, 434, 1039.
 Charnley S. B. et al. (1992) *Astrophys. J.*, 399, L71.
 Chatterjee S. and Tan J. C. (2012) *Astrophys. J.*, 754, 152.
 Chen H.-R., Liu S.-Y., Su Y. et al. (2011) *Astrophys. J.*, 743, 196.
 Chen X., Shen Z.-Q., Li Ji.-J. et al. (2010) *Astrophys. J.*, 710, 150.
 Chini R., Hoffmeister V. et al. (2004) *Nature*, 429, 155.
 Chira R.-A. et al. (2013) *Astron. Astrophys.*, 552, 40.
 Churchwell E., Babler B., Meade M. et al. (2009) *PASP*, 121, 213.
 Clark P. C. et al. (2007) *Mon. Not. R. Astron. Soc.*, 379, 57.
 Codella C. et al. (2013) *Astron. Astrophys.*, 550, 81.
 Commerçon B. et al. (2011a) *Astrophys. J.*, 742, L9.
 Commerçon B. et al. (2011b) *Astron. Astrophys.*, 529, 35.
 Crapsi A., Caselli P. et al. (2005) *Astrophys. J.*, 619, 379.
 Crowther P. A. et al. (2010) *Mon. Not. R. Astron. Soc.*, 408, 731.
 Crutcher R. M. (2012) *Annu. Rev. Astron. Astrophys.*, 50, 29.
 Cunningham A. J. et al. (2011) *Astrophys. J.*, 740, 107.
 Da Rio N., Robberto M. et al. (2012) *Astrophys. J.*, 748, 14.
 Dale J. E. et al. (2005) *Mon. Not. R. Astron. Soc.*, 358, 291.
 Dalgarno A. (2006) *Proc. Nat. Acad. of Sci.*, 103, 12269.
 Dalgarno A. and Lepp S. (1984) *Astrophys. J.*, 287, L47.
 Davies B. et al. (2011) *Mon. Not. R. Astron. Soc.*, 416, 972.
 Davies B. et al. (2010) *Mon. Not. R. Astron. Soc.*, 402, 1504.
 De Buizer J. M. (2006) *Astrophys. J.*, 642, L57.
 de Gouveia Dal Pino E. et al. (2012) *Physica Scripta*, 86, 018401.
 de Mink S. E., Langer N. et al. (2013) *Astrophys. J.*, 764, 166.
 de Wit W. J. et al. (2011) *Astron. Astrophys.*, 526, L5.
 de Wit W. J., Testi L. et al. (2005) *Astron. Astrophys.*, 437, 247.
 Demyk K., Bottinelli S. et al. (2010) *Astron. Astrophys.*, 517, 17.
 Dobbs C. L. et al. (2005) *Mon. Not. R. Astron. Soc.*, 360, 2.
 Draine B. T. (2011) *Physics of the Interstellar and Intergalactic Medium* (Princeton: Princeton Univ. Press)
 Duarte-Cabral A. et al. (2013) *Astron. Astrophys.*, 558, 125.
 Duffin D. F. and Pudritz R. E. (2008) *Mon. Not. R. Astron. Soc.*, 391, 1659.
 Edgar R. and Clarke C. (2004) *Mon. Not. R. Astron. Soc.*, 349, 678.
 Ellingsen S. P., Voronkov M. A. et al. (2007) *IAU Symp.*, 242, 213.
 Emprechtinger M. et al. (2009) *Astron. Astrophys.*, 493, 89.
 Emprechtinger M., Lis D. C. et al. (2013) *Astrophys. J.*, 765, 61.
 Falgarone E. et al. (2008) *Astron. Astrophys.*, 487, 247.
 Fatuzzo M. and Adams F. C. (2002) *Astrophys. J.*, 570, 210.
 Favre C., Despois D. et al. (2011) *Astron. Astrophys.*, 532, 32.
 Fernández-López M., Girart J. M. et al. (2011) *Astron. J.*, 142, 97.
 Fiege J. D. and Pudritz R. E. (2000) *Mon. Not. R. Astron. Soc.*, 311, 85.
 Figer D. F. (2005) *Nature*, 434, 192.
 Fontani F., Caselli P. et al. (2008) *Astron. Astrophys.*, 477, L45.
 Fontani F. et al. (2012) *Mon. Not. R. Astron. Soc.*, 423, 2342.
 Fontani F., Palau A. et al. (2011) *Astron. Astrophys.*, 529, L7.
 Foster J. B. et al. (2009) *Astrophys. J.*, 696, 298.
 Franco-Hernández R. et al. (2009) *Astrophys. J.*, 701, 974.
 Fryxell B., Olson K. et al. (2000) *Astrophys. J. Suppl.*, 131, 273.
 Fuente A. et al. (2009) *Astron. Astrophys.*, 507, 1475.
 Fuente A., Caselli P. et al. (2012) *Astron. Astrophys.*, 540, 75.

- Fuller G. A. et al. (2005) *Astron. Astrophys.*, 442, 949.
- Garay G., Mardones D. et al. (2007) *Astron. Astrophys.*, 463, 217.
- Garrod R. T. (2013) *Astrophys. J.*, 765, 60.
- Garrod R. T. and Herbst E. (2006) *Astron. Astrophys.*, 457, 927.
- Gibb A. G. et al. (2003) *Mon. Not. R. Astron. Soc.*, 339, 198.
- Ginsburg A., Bressert E. et al. (2012) *Astrophys. J.*, 758, L29.
- Girart J., Beltrán M., Zhang Q. et al. (2009) *Science*, 324, 1408.
- Girichidis P. et al. (2012) *Mon. Not. R. Astron. Soc.*, 420, 613.
- Goddi C. et al. (2011a) *Astron. Astrophys.*, 535, L8.
- Goddi C., Humphreys E. et al. (2011b) *Astrophys. J.*, 728, 15.
- Greenhill L. J., Goddi C. et al. (2013) *Astrophys. J.*, 770, L32.
- Guzmán A. E., Garay G. et al. (2010) *Astrophys. J.*, 725, 734.
- Habibi M., Stolte A. et al. (2013) *Astron. Astrophys.*, 556, 26.
- Haemmerlé L. et al. (2013) *Astron. Astrophys.*, 557, 112.
- Harfst S. et al. (2010) *Mon. Not. R. Astron. Soc.*, 409, 628.
- Hennebelle P. et al. (2011) *Astron. Astrophys.*, 528, 72.
- Henning Th., Linz H. et al. (2010) *Astron. Astrophys.*, 518, L95.
- Henshaw J. et al. (2013) *Mon. Not. R. Astron. Soc.*, 428, 3425.
- Herbst E. and van Dishoeck E. F. (2009) *Ann. Rev. Astron. Astrophys.*, 47, 427.
- Hernandez A. K., Tan J. C. et al. (2012) *Astrophys. J.*, 756, L13.
- Herpin F., Chavarría L., et al. (2012) *Astron. Astrophys.*, 542, 76.
- Heyer M. H., Krawczyk C. et al. (2009) *Astrophys. J.*, 699, 1092.
- Hillenbrand L. A., Meyer M. R. et al. (1995) *Astron. J.*, 109, 280.
- Hoare M. G., Kurtz S. E., Lizano S. et al. (2007) *PPV* (B. Reipurth et al.), Univ. Arizona, Tucson, p181-196.
- Hofner P., Cesaroni R. et al. (2007) *Astron. Astrophys.*, 465, 197.
- Hollenbach D., Johnstone D. et al. (1994) *Astrophys. J.*, 428, 654.
- Hoogerwerf R. et al. (2001) *Astron. Astrophys.*, 365, 49.
- Hosokawa T. and Omukai K. (2009) *Astrophys. J.*, 691, 823.
- Hosokawa T., Omukai K. et al. (2011) *Science*, 334, 1250.
- Hosokawa T., Yorke H. W. et al. (2010) *Astrophys. J.*, 721, 478.
- Houde M., Phillips, T., Vaillancourt J. et al. (2009) *Sub-mm Astrophysics & Tech.* (D. Lis et al.), *ASP Conf. Ser.*, 417, 265.
- Hunter C. (1977) *Astrophys. J.*, 218, 834.
- Hunter T., Testi L., Zhang Q. et al. (1999) *Astrophys. J.*, 118, 477.
- Hußmann B., Stolte A. et al. (2012) *Astron. Astrophys.*, 540, 57.
- Ilee J. D. et al. (2013) *Mon. Not. R. Astron. Soc.*, 429, 2960.
- Jiang Y.-F., Davis S. W. et al. (2013) *Astrophys. J.*, 763, 102.
- Jijina J. and Adams F. C. (1996) *Astrophys. J.*, 462, 874.
- Jiménez-Serra I., Caselli P., Tan J. C. et al. (2010) *Mon. Not. R. Astron. Soc.*, 406, 187.
- Johnston K. G. et al. (2011) *Mon. Not. R. Astron. Soc.*, 415, 2952.
- Kahn F. D. (1974) *Astron. Astrophys.*, 37, 149.
- Kainulainen J. and Tan J. C. (2013) *Astron. Astrophys.*, 549, 53.
- Kalvāns J. and Shmeld I. (2013) *Astron. Astrophys.*, 554, 111.
- Kauffmann J., Pillai T. et al. (2010) *Astrophys. J.*, 716, 433.
- Keto E. (2002) *Astrophys. J.*, 568, 754.
- Keto E. (2007) *Astrophys. J.*, 666, 976.
- Keto E. and Caselli P. (2010) *Mon. Not. R. Astron. Soc.*, 402, 1625.
- Keto E. and Klaassen P. D. (2008) *Astrophys. J.*, 678, L109.
- Kirk H. and Myers P. C. (2012) *Astrophys. J.*, 745, 131.
- Klaassen P. D., Testi L. et al. (2012) *Astron. Astrophys.*, 538, 140.
- Königl A. and Pudritz R. E. (2000) *Protostars and Planets IV*, 759.
- Kratter K. M. et al. (2010) *Astrophys. J.*, 708, 1585.
- Kraus S., Hofmann K., Menten K. et al. (2010) *Nature*, 466, 339.
- Krumholz M. R. (2014) *Physics Rep.*, in press, arXiv1402.0867.
- Krumholz M. R., Klein R. I. et al. (2007a) *Astrophys. J.*, 656, 959.
- Krumholz M. R., Klein R. I. et al. (2007c) *Astrophys. J.*, 665, 478.
- Krumholz M. R., Klein R. I. et al. (2012) *Astrophys. J.*, 754, 71.
- Krumholz M. R., Klein R. I. et al. (2007b) *Astrophys. J.*, 667, 626.
- Krumholz M. R., Klein R. I. et al. (2009) *Science*, 323, 754.
- Krumholz M. R. and McKee C. F. (2008) *Nature*, 451, 1082.
- Krumholz M. R., McKee C. et al. (2004) *Astrophys. J.*, 611, 399.
- Krumholz M. R., McKee C. F. et al. (2005a) *Nature*, 438, 332.
- Krumholz M. R., McKee C. et al. (2005b) *Astrophys. J.*, 618, L33.
- Krumholz M. R. and Tan J. C. (2007) *Astrophys. J.*, 654, 304.
- Kuiper R., Klahr H. et al. (2010a) *Astrophys. J.*, 722, 1556.
- Kuiper R., Klahr H. et al. (2011) *Astrophys. J.*, 732, 20.
- Kuiper R., Klahr H. et al. (2012) *Astron. Astrophys.*, 537, 122.
- Kuiper R., Klahr H. et al. (2010b) *Astron. Astrophys.*, 511, 81.
- Kuiper R. and Yorke H. W. (2013) *Astrophys. J.*, 763, 104.
- Kumar M. S. N. et al. (2006) *Astron. Astrophys.*, 449, 1033.
- Kunz M. W. and Mouschovias T. Ch. (2009) *Mon. Not. R. Astron. Soc.*, 399, L94.
- Lacy J. H., Knacke R. et al. (1994) *Astrophys. J.*, 428, L69.
- Lada C. J. (1991) *The Physics of Star Formation and Early Stellar Evolution* (C. Lada and N. Kylafis), Kluwer, Dordrecht, p329.
- Larsen S. S. et al. (2008) *Mon. Not. R. Astron. Soc.*, 383, 263.
- Larson R. B. (1985) *Mon. Not. R. Astron. Soc.*, 214, 379.
- Larson R. B. and Starrfield S. (1971) *Astron. Astrophys.*, 13, 190.
- Leurini S., Codella C. et al. (2013) *Astron. Astrophys.*, 554, 35.
- Li P. S., Martin D., Klein R. et al. (2012a) *Astrophys. J.*, 745, 139.
- Li P. S., McKee C. F., and Klein R. (2012b) *Astrophys. J.*, 744, 73.
- Lim B., Chun M.-Y., Sung H. et al. (2013) *Astron. J.*, 145, 46.
- Longmore S. N., Pillai T. et al. (2011) *Astrophys. J.*, 726, 97.
- Longmore S. N. et al. (2012) *Astrophys. J.*, 746, 117.
- López-Sepulcre A. et al. (2010) *Astron. Astrophys.*, 517, 66.
- López-Sepulcre A. et al. (2009) *Astron. Astrophys.*, 499, 811.
- López-Sepulcre A. et al. (2011) *Astron. Astrophys.*, 526, L2.
- Lu J. R., Do T., Ghez A. M. et al. (2013) *Astrophys. J.*, 764, 155.
- Lucy L. B. (1977) *Astron. J.*, 82, 1013.
- Lumsden S. L. et al. (2012) *Mon. Not. R. Astron. Soc.*, 424, 1088.
- Lumsden S. L. et al. (2013) *Astrophys. J. Suppl.*, 208, 11.
- Mardones D., Myers P. C. et al. (1997) *Astrophys. J.*, 489, 719.
- Maschberger Th. and Clarke C. J. (2011) *Mon. Not. R. Astron. Soc.*, 416, 541.
- Matthews B. C. et al. (2009) *Astrophys. J. Suppl.*, 182, 143.
- Matzner C. D. (2007) *Astrophys. J.*, 659, 1394.
- Matzner C. D. and McKee C. F. (1999) *Astrophys. J.*, 526, L109.
- Matzner C. D. and McKee C. F. (2000) *Astrophys. J.*, 545, 364.
- McCrary N. and Graham J. R. (2007) *Astrophys. J.*, 663, 844.
- McKee C. F. (1989) *Astrophys. J.*, 345, 782.
- McKee C. F. and Hollimann, J. H. (1999) *Astrophys. J.*, 522, 313.
- McKee C. F. and Ostriker E. C. (2007) *Ann. Rev. Astron. Astrophys.* 45, 565.
- McKee C. F., Li P. and Klein R. (2010), *Astrophys. J.*, 720, 1612.
- McKee C. F. and Tan J. C. (2002) *Nature*, 416, 59.
- McKee C. F. and Tan J. C. (2003) *Astrophys. J.*, 585, 850. [MT03]
- McKee C. F. and Tan J. C. (2008) *Astrophys. J.*, 681, 771.
- McKee C. F. and Williams J. P. (1997) *Astrophys. J.*, 476, 144.
- Menten K. M. and Reid M. J. (1995) *Astrophys. J.*, 445, L157.
- Miettinen O. et al. (2011) *Astron. Astrophys.*, 534, 134.
- Moeckel N. and Clarke C. J. (2011) *Mon. Not. R. Astron. Soc.*, 410, 2799.
- Molinari S., Pezzuto S. et al. (2008) *Astron. Astrophys.*, 481, 345.
- Morino J.-I., Yamashita T. et al. (1998) *Nature*, 393, 340.
- Morris M. and Serabyn E. (1996) *Ann. Rev. Astron. Astrophys.* 34, 645.
- Moscadelli L., Li J. J. et al. (2013) *Astron. Astrophys.*, 549, 122.
- Mottram J. C., Hoare M. G. et al. (2011) *Astrophys. J.*, 730, L33.
- Mouschovias T. Ch. (1987) *Physical Processes in Interstellar Clouds* (G. Morfill & M. Scholer), Dordrecht, Reidel, 453.
- Mueller K. E. et al. (2002), *Astrophys. J. Suppl.*, 143, 469.
- Myers A. T., McKee C. F. et al. (2013) *Astrophys. J.*, 766, 97.
- Myers P. C. and Fuller G. A. (1992) *Astrophys. J.*, 396, 631.
- Najita J. R. and Shu F. H. (1994) *Astrophys. J.*, 429, 808.
- Nakano T. (1989) *Astrophys. J.*, 345, 464.
- Neill J., Wang S., Bergin E. et al. (2013) *Astrophys. J.*, 770, 142.
- Neufeld D. A. and Dalgarno A. (1989) *Astrophys. J.*, 340, 869.
- Öberg K. I., Boogert A. et al. (2011) *Astrophys. J.*, 740, 109.
- Öberg K. I., Boamah M. et al. (2013) *Astrophys. J.*, 771, 95.
- Oey M. S., Lamb J. B. et al. (2013) *Astrophys. J.*, 768, 66.
- Ossenkopf V. and Henning T. (1994) *Astron. Astrophys.*, 291, 943.
- Padoan P. and Nordlund A. (2007) *Astrophys. J.*, 661, 972.

- Padovani M. and Galli D. (2011) *Astron. Astrophys.*, 530, 109.
- Palau A., Fuente A., Girart J. et al. (2011) *Astrophys. J.*, 743, L32.
- Palau A., Fuente A., Girart J. et al. (2013) *Astrophys. J.*, 762, 120.
- Palla F. and Stahler S. W. (1991) *Astrophys. J.*, 375, 288.
- Pang X., Grebel E., Allison R. et al. (2013) *Astrophys. J.*, 764, 73.
- Parker R. J. et al. (2011) *Mon. Not. R. Astron. Soc.*, 418, 2565.
- Patel N. A., Curiel S., Sridharan T. et al. (2005) *Nature*, 437, 109.
- Paumard T., Genzel R. et al. (2006) *Astrophys. J.*, 643, 1011.
- Peretto N. and Fuller G. A. (2009) *Astron. Astrophys.*, 505, 405.
- Peretto N., Fuller G. et al. (2013), *Astron. Astrophys.*, 555, 112.
- Peretto N., Fuller G. et al. (2010) *Astron. Astrophys.*, 518, L98.
- Pestalozzi M. R. et al. (2009) *Astron. Astrophys.*, 501, 999.
- Peters T., Banerjee R. et al. (2010a) *Astrophys. J.*, 711, 1017.
- Peters T., Banerjee R. et al. (2011) *Astrophys. J.*, 729, 72.
- Peters T., Klessen R. S. et al. (2010b) *Astrophys. J.*, 725, 134.
- Pillai T., Kauffmann J. et al. (2011) *Astron. Astrophys.*, 530, 118.
- Pillai T., Wyrowski F. et al. (2006) *Astron. Astrophys.*, 450, 569.
- Plambeck R. L., Bolatto A. D. et al. (2013) *Astrophys. J.*, 765, 40.
- Plume R., Jaffe D., Evans N. et al. (1997) *Astrophys. J.*, 476, 730.
- Preibisch T., Ratzka T. et al. (2011) *Astron. Astrophys.*, 530, 40.
- Price D. J. and Monaghan J. J. (2004) *Mon. Not. R. Astron. Soc.*, 348, 123.
- Qiu K., Zhang Q. et al. (2012) *Astrophys. J.*, 756, 170.
- Qiu K., Zhang Q. et al. (2007) *Astrophys. J.*, 654, 361.
- Qiu K., Zhang Q. et al. (2008) *Astrophys. J.*, 685, 1005.
- Ragan S. E., Bergin E. A. et al. (2009) *Astrophys. J.*, 698, 324.
- Ragan S. E. et al. (2012) *Astron. Astrophys.*, 547, 49.
- Rathborne J. M. et al. (2006) *Astrophys. J.*, 641, 389.
- Reid M. J., Argon A. L. et al. (1995) *Astrophys. J.*, 443, 238.
- Robitaille T. P. et al. (2006) *Astrophys. J. Suppl.*, 167, 256.
- Rodón J. A. et al. (2012) *Astron. Astrophys.*, 545, 51.
- Roman-Duval J. et al. (2010) *Astrophys. J.*, 723, 492.
- Rosen A. L., Krumholz M. R. et al. (2012) *Astrophys. J.*, 748, 97.
- Sabbi E., Sirianni M., Nota A. et al. (2008) *Astron. J.*, 135, 173.
- Sakai T., Sakai N., Furuya K. et al. (2012) *Astrophys. J.*, 742, 140.
- Sakai T., Sakai N. et al. (2008) *Astrophys. J.*, 678, 1049.
- San José-García I. et al. (2013) *Astron. Astrophys.*, 553, 125.
- Sana H., de Mink S., de Koter A. et al. (2012) *Science*, 337, 444.
- Sánchez-Monge Á. et al. (2013a) *Astron. Astrophys.*, 552, L10.
- Sánchez-Monge Á. et al. (2013b), *Astron. Astrophys.*, 552, L10.
- Sánchez-Monge Á., Palau A., Fontani F. et al. (2013c) *Mon. Not. R. Astron. Soc.*, 432, 3288.
- Sanhueza P., Jackson J. M. et al. (2013) *Astrophys. J.*, 773, 123.
- Santangelo G., Testi L. et al. (2009) *Astron. Astrophys.*, 501, 495.
- Schneider F. R. N., Izzard R. et al. (2014) *Astrophys. J.*, 780, 117.
- Schneider N. et al. (2010) *Astron. Astrophys.*, 520, 49.
- Selier R. et al. (2011) *Astron. Astrophys.*, 529, 40.
- Sewilo M. et al. (2011) *Astrophys. J. Suppl.*, 194, 44.
- Shu F. H. (1977) *Astrophys. J.*, 214, 488.
- Shu F. H. et al. (1987) *Ann. Rev. Astron. Astrophys.*, 25, 23.
- Shu F. H., Najita J. R., Shang S., and Li Z.-Y. (2000) *Protostars and Planets IV*, (V. Mannings), Tucson, Univ. Arizona, 789.
- Smith R. J. et al. (2011) *Mon. Not. R. Astron. Soc.*, 411, 1354.
- Smith R. J. et al. (2009) *Mon. Not. R. Astron. Soc.*, 400, 1775.
- Smith R. J., Shetty R. et al. (2013) *Astrophys. J.*, 771, 24.
- Sollins P., Hunter T., and Battat J. (2004) *Astrophys. J.*, 616, L35.
- Sollins P., Zhang Q., Keto E. et al. (2005) *Astrophys. J.*, 624, L49.
- Solomon P. M., Rivolo A. R. et al. (1987) *Astrophys. J.*, 319, 730.
- Sridharan T. K. et al. (2014) *Astrophys. J.*, 783, L31.
- Su Y.-N., Liu S.-Y., Chen H. et al. (2012) *Astrophys. J.*, 744, L26.
- Suttner G., Yorke H., and Lin D. (1999) *Astrophys. J.*, 524, 857.
- Tan J. C. (2004) *Astrophys. J.*, 607, L47.
- Tan J. C., Krumholz, M. R. et al. (2006) *Astrophys. J.*, 641, L121.
- Tan J. C. and McKee C. F. (2003) astro-ph/0309139.
- Tan J. C. and McKee C. F. (2004) *Astrophys. J.*, 603, 383.
- Tan J. C., Shaske S., and Van Loo S. (2013a) *IAU Symp.*, 292, 19.
- Tan J. C., Kong S. et al. (2013b) *Astrophys. J.*, 779, 76.
- Tanaka K. E. I. and Nakamoto T. (2011) *Astrophys. J.*, 739, L50.
- Tanaka K. E. I., Nakamoto T. et al. (2013) *Astrophys. J.*, 773, 155.
- Tang Y.-W. et al. (2009) *Astrophys. J.*, 700, 251.
- Taquet V., Peters P. S. et al. (2013) *Astron. Astrophys.*, 550, 127.
- Testi L., Tan J. C. and Palla F. (2010) *Astron. Astrophys.*, 522, 44.
- Torstensson K. J. E. et al. (2011) *Astron. Astrophys.*, 529, 32.
- Turner J. L., and Beck S. C. (2004) *Astrophys. J.*, 602, L85.
- Urban A., Martel H. and Evans N. (2010) *Astrophys. J.*, 710, 1343.
- Vaidya B. et al. (2011) *Astrophys. J.*, 742, 56.
- van der Tak F. F. S. et al. (2010) *Astron. Astrophys.*, 518, L107.
- van der Wiel M. H. D. et al. (2013) *Astron. Astrophys.*, 553, 11.
- Vasyunina T., Vasyunin A. I. et al. (2012) *Astrophys. J.*, 751, 105.
- Vink J. S., de Koter A. et al. (2001) *Astron. Astrophys.*, 369, 574.
- Viti S. et al. (2004) *Mon. Not. R. Astron. Soc.*, 354, 1141.
- Vlemmings W. et al. (2010) *Mon. Not. R. Astron. Soc.*, 404, 134.
- Wang K.-S. et al. (2012) *Astron. Astrophys.*, 543, 22.
- Wang P., Li Z., Abel T. et al. (2010) *Astrophys. J.*, 709, 27.
- Wang Y., Zhang Q., Pillai, T. et al. (2008) *Astrophys. J.*, 672, L33.
- Weidner C. et al. (2013) *Mon. Not. R. Astron. Soc.*, 434, 84.
- Werner M. W., Capps R. W. et al. (1983) *Astrophys. J.*, 265, L13.
- Whitehouse S. C. and Bate M. R. (2004) *Mon. Not. R. Astron. Soc.*, 353, 1078.
- Williams J. P. and Garland C. A. (2002) *Astrophys. J.*, 568, 259.
- Wolfire M. G. and Cassinelli J. (1987) *Astrophys. J.*, 319, 850.
- Wood D. O. S. and Churchwell E. (1989) *Astrophys. J.*, 340, 265.
- Wu J. and Evans N. J. (2003) *Astrophys. J.*, 592, L79.
- Wu Y., Qin S.-L., Guan X. et al. (2009) *Astrophys. J.*, 697, L116.
- Wu Y., Zhang Q., Chen H. et al. (2005a) *Astron. J.*, 129, 330.
- Wu Y., Zhu M., Wei Y. et al. (2005b) *Astrophys. J.*, 628, L57.
- Wyrowski F. et al. (2012) *Astron. Astrophys.*, 542, L15.
- Yıldız U. A. et al. (2013) *Astron. Astrophys.*, 556, 89.
- Yorke H. and Sonnhalter C. (2002) *Astrophys. J.*, 569, 846.
- Zapata L. A., Palau A., Ho P. et al. (2008) *Astrophys. J.*, 479, L25.
- Zapata L. A. et al. (2013) *Astrophys. J.*, 765, L29.
- Zhang Q., Sridharan T. K. et al. (2007) *Astrophys. J.*, 470, 269.
- Zhang Q., Wang Y., Pillai T. et al. (2009) *Astrophys. J.*, 696, 268.
- Zhang Y. and Tan J. C. (2011) *Astrophys. J.*, 733, 55.
- Zhang Y., Tan J. C. et al. (2013a) *Astrophys. J.*, 766, 86.
- Zhang Y., Tan J. C. et al. (2013b) *Astrophys. J.*, 767, 58.
- Zhang Y., Tan J. C. et al. (2014) *Astrophys. J.*, 788, 166.
- Zinnecker H. and Yorke H. (2007) *Ann. Rev. Astron. Astrophys.* 45, 481.

Massive Star Formation paper fails to recognize that dark matter planets dominate the mass of "giant molecular cloud" PGCs

Massive Star Formation

Jonathan C. Tan¹, Maria T. Beltrán², Paola Caselli³, Francesco Fontani², Asunción Fuente⁴, Mark R. Krumholz⁵, Christopher F. McKee⁶, Andrea Stolte⁷

¹University of Florida; ²INAF-Osservatorio Astrofisico di Arcetri; ³University of Leeds; ⁴Osservatorio Astronomico Nazionale; ⁵University of California, Santa Cruz; ⁶University of California, Berkeley; ⁷Argelander Institut für Astronomie, Universität Bonn

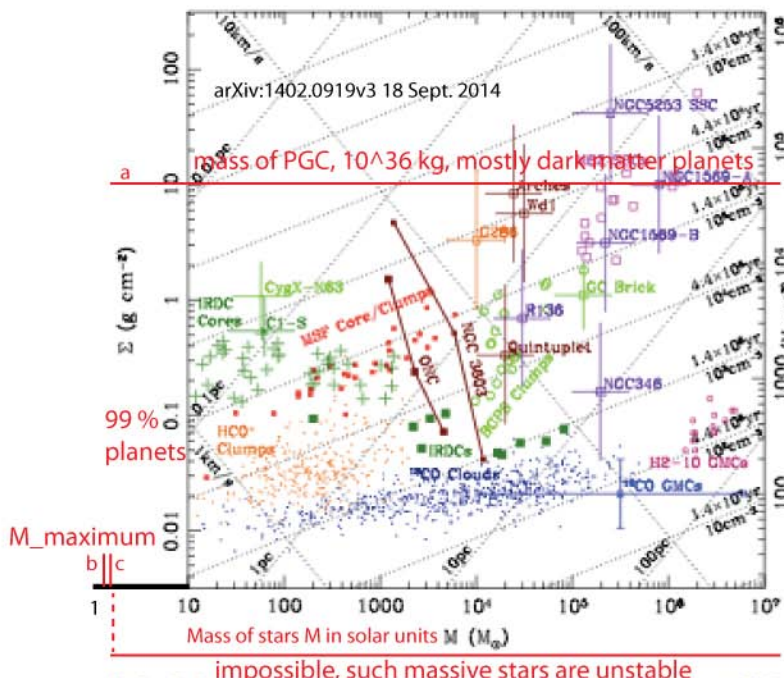


Fig. 1.— The Environment of Massive Star Formation. Mass surface density, $\Sigma \equiv M/(\pi R^2)$, is plotted versus mass, M . Dotted lines of constant radius, R , H number density, n_0 for free-fall time, $t_0 = (3\pi/32G\rho_0)^{1/2} R$, and escape speed, $v_{\text{esc}} = (10/\pi n_0)^{1/2} v_0$, are shown. Stars form from molecular gas, which in the Galaxy is mostly organized into GMCs. Typical ^{13}CO -detected GMCs have $\Sigma \sim 100 M_{\odot} \text{pc}^{-2}$ (Siverton et al. 1987) (see Tan et al. 2013a for detailed discussion of the methods for estimating Σ for the objects plotted here, although denser examples have been found in Henric 2, 10 (Siverton et al. 2009). The ^{13}CO -detected clouds of Rosenbluth et al. (2010) are indicated, along with HCO^+ clumps of Krumholz et al. (2011), including G286.21+0.17 (Krumholz et al. 2010). Along with G281, the IRDCs clumps (Gouvy et al. 2012) and the Galactic Center “Brick” (Lungwiler et al. 2012) are some of the most massive, high Σ gas clumps known in the Milky Way. Ten example Infrared Dark Clouds (IRDCs) (Kawamura and Tan 2013) and their internal core/clumps (Riadler and Tan 2012) are shown, including the massive, molecular, highly-luminous core C1-S (Tan et al. 2013b). CygX-N63, a core with similar mass and size as C1-S, appears to be forming a single massive protostar (Bouwman et al. 2010; Dunne-Gabell et al. 2013). The IRDC core/clumps overlap with Massive Star-Forming (MSF) core/clumps (Mueller et al. 2002). Clumps may give rise to young star clusters, like the ONC (e.g., Zhu Liu et al. 2012) and NGC 3603 (Pang et al. 2013) (radial structure is shown from core to half-mass, $R_{0.5}$, to outer radius), or even more massive examples, e.g., Westerlund 1 (Liu et al. 2013). Anches (Wafahi et al. 2013), Quintuplet (Wegmann et al. 2012) (shown at $R_{1/2}$), that are in the regime of “super star clusters” (SSCs), i.e., with $M_* \geq 10^4 M_{\odot}$. Example SSCs is the Large Magellanic Cloud (LMC) (R136, Anderson et al. 2009) and Small Magellanic Cloud (SMC) (NGC 346, Sabbi et al. 2008) display a wide range of Σ , but no evidence of IMF variation (§5.2). Even more massive clusters can be found in some dwarf irregular galaxies, such as NGC 1569 (Larsen et al. 2006) and NGC 5253 (Fox and Beck 2004), and starburst galaxy M82 (McCreadly and Goshokan 2007).

HGD cosmology shows: all ProtoGlobalCluster clumps of dark matter planets weigh 10^{36} kg, the maximum mass OBA star weighs 1.3 solar, the maximum mass carbon star weighs 1.4 solar.

Hydro-Gravitational-Dynamics Cosmology
Primordial-Fog-Particles in Proto-Globular-Clusters
Plasma Proto-Galaxies on turbulent vortex lines
Big Bang turbulent combustion at Planck scales

New
Cosmology

Massive Stars are
obsolete:HGD

Solar mass primordial black holes

Nobel Prize in Physics 2011

Accelerating expansion of the Universe

Turbulence that cascades from large scales to small

Irrotational Fluid Mechanics

Inviscid Fluid Mechanics

Collisionless Fluid Mechanics

Self Interacting Dark Matter

Dark Ages

Reionization

Cold Dark Matter

Hierarchical Clustering

Old
Cosmology

Λ

